

# Uplift Resistance of Anchor Plate Using Extended Mohr-Coulomb Model



Kyeong Sun Kim

Civil and Environmental Engineering

Seoul National University

November, 2021

# Contents

|  |           |
|--|-----------|
| <b>1 Constitutive Model</b>  | <b>2</b>  |
| 1.1 Strain—Softening Stiffness—Hardening Model . . . . .                                       | 3         |
| 1.1.1 Yield function . . . . .   | 3         |
| 1.1.2 Plastic potential function . . . . .   | 3         |
| 1.1.3 Hardening function . . . . .   | 4         |
| 1.2 Nonassociated Flow Rule (NA) . . . . .   | 5         |
| 1.3 Extended Mohr—Coulomb Model (EMC) . . . . .  | 7         |
| 1.3.1 Comparison between associated and non-associated flow rule<br>in plastic model . . . . . | 8         |
| 1.3.2 Yield function . . . . .   | 9         |
| 1.3.3 Plastic potential function . . . . .   | 9         |
| 1.3.4 Flow rule . . . . .  | 10        |
| 1.3.5 Hardening . . . . .  | 10        |
| 1.3.6 Soil Parameters . . . . .  | 10        |
| <b>2 Calibration and Validation</b>  | <b>12</b> |
| 2.1 Drained Triaxial Test . . . . .  | 13        |
| 2.2 Soil Parameters . . . . .  | 16        |
| 2.2.1 Strain—Softening Stiffness—Hardening Model . . . . .                                     | 16        |
| 2.2.2 Nonassociated Flow Rule (NA) . . . . .   | 16        |
| 2.2.3 Extended Mohr—Coulomb Model (EMC) . . . . .  | 17        |
| 2.3 Convergence Criteria . . . . .   | 18        |
| 2.3.1 Mesh Convergence . . . . .   | 18        |
| 2.3.2 Boundary Convergence . . . . .   | 25        |
| <b>3 Results</b>   | <b>28</b> |
| 3.1 Parametric Study . . . . .   | 28        |
| 3.1.1 Effect of Embedment Depth Ratio $\frac{D}{B}$ . . . . .                                  | 31        |

*Contents*

|                   |   |           |
|-------------------|---|-----------|
| 3.1.2             | Effect of Width $B$ . . . . .                                       | 32        |
| 3.1.3             | Shear Dissipation . . . . .   | 32        |
| 3.2               | Comparison with Previous Researchers . . . . .                      | 39        |
| <b>4</b>          | <b>Comparison with Centrifuge Experiment</b>                        | <b>41</b> |
| 4.1               | Comparison of the centrifuge test results with the chosen model . . | 53        |
| <b>Appendices</b> |   |           |
| <b>A</b>          | <b>List of Load—Displacement Curves</b>                             | <b>56</b> |
| <b>B</b>          | <b>REFERENCES</b>   | <b>63</b> |

## Contents

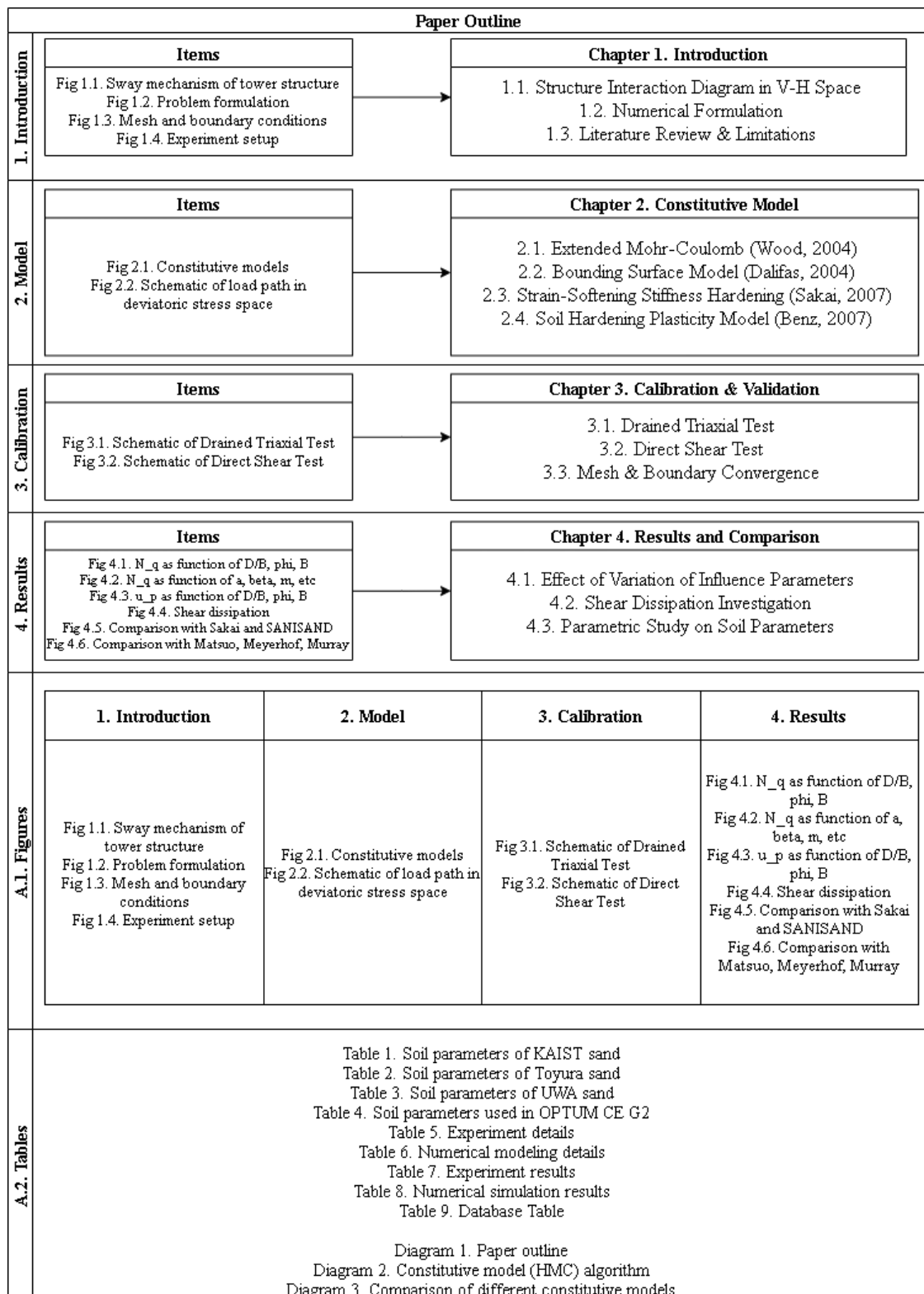


**Figure 1:** Paper Outline

# 1

## Constitutive Model

### Contents

---

|            |   |          |
|------------|---|----------|
| <b>1.1</b> | <b>Strain—Softening Stiffness—Hardening Model . . . . .</b>                           | <b>3</b> |
| 1.1.1      | Yield function . . . . .  | 3        |
| 1.1.2      | Plastic potential function . . . . .  | 3        |
| 1.1.3      | Hardening function . . . . .  | 4        |
| <b>1.2</b> | <b>Nonassociated Flow Rule (NA) . . . . .</b>   | <b>5</b> |
| <b>1.3</b> | <b>Extended Mohr—Coulomb Model (EMC) . . . . .</b>                                    | <b>7</b> |
| 1.3.1      | Comparison between associated and non-associated flow rule in plastic model . . . . . | 8        |
| 1.3.2      | Yield function . . . . .  | 9        |
| 1.3.3      | Plastic potential function . . . . .  | 9        |
| 1.3.4      | Flow rule . . . . .   | 10       |
| 1.3.5      | Hardening . . . . .   | 10       |
| 1.3.6      | Soil Parameters . . . . .   | 10       |

---

## 1. Constitutive models

Here is a brief description of the constitutive models:

1. Strain—Softening Stiffness—Hardening Model by Sakai and Tanaka, 1993
2. Typical Mohr-Coulomb with Non-associated Flow
3. Extended Mohr-Coulomb Model by David Muir Wood, 2004

### 1.1 Strain—Softening Stiffness—Hardening Model

It is assumed that the yield function  $F$  is defined by the stress  $\vec{\sigma}$  and the soil parameter  $\chi$  (Tanaka and Sakai, 1993):

$$F(\vec{\sigma}, \alpha(\chi)) = 0$$

In order to avoid numerical instability due to singularity of the non-associated Mohr-Coulomb model, a constitutive model based on the yield function of M-C type and the plastic potential function of Draker-Prager type is employed.

For predicting deformations in a post-peak regime, the elastic- strain-softening plastic model is developed. The yield function is given by the following expression.

#### 1.1.1 Yield function

$$F(\vec{\sigma}, \alpha(\chi)) = 3\alpha(\chi)p' + \frac{\sqrt{J_2}}{g(\theta)} - c(\chi) = 0$$

#### 1.1.2 Plastic potential function

$$G(\vec{\sigma}, \alpha'(\chi)) = 3\alpha'(\chi)p' + \sqrt{J_2} - c(\chi) = 0$$

$$\chi = \int \delta \varepsilon^p$$

$$(\delta \varepsilon^p)^2 = 2[(\delta \epsilon_x^p)^2 + (\delta \epsilon_y^p)^2 + (\delta \epsilon_z^p)^2] + (\delta \gamma^p)^2$$

, where

$p'$  is mean stress,

$J_2$  is second invariant of deviatoric stress,

## 1. Constitutive models

$\chi$  is soil hardening parameter,

$c(\chi)$  is apparent cohesion function,

$\delta\varepsilon_{x,y,z}^p, \delta\gamma^p$  is incremental deviatoric plastic strains.

In case of the Mohr-Coulomb model,  $g(\theta)$  is given by:

$$g(\theta) = \frac{3 - \sin\phi}{2\sqrt{3}\cos\theta - 2\sin\theta\sin\phi}$$

, where

$\theta$  is Lode angle; if triaxial compression,  $= -30^\circ$

$\phi$  is mobilized internal friction angle.

### 1.1.3 Hardening function

The simple strain-softening functions are specified and expressed as a function of material constants. (Tanaka and Sakai, 1993)

$$\alpha(\chi) = \left( \frac{2\sqrt{a\chi}}{\chi + a} \right)^m \alpha_p \text{(hardening regime; } \chi \leq a)$$

$$\alpha(\chi) = \alpha_r + (\alpha_p - \alpha_r) \exp\left\{-\left(\frac{\chi - a}{b}\right)\right\} \text{(softening regime; } \chi > a)$$

, where

$a, b, m$  are soil parameters.

Similar expressions are used by de Borst (1986).

$$\alpha_p = \frac{2\sin\phi_p}{\sqrt{3}(3 - \sin\phi_p)}$$

$$\alpha_r = \frac{2\sin\phi_r}{\sqrt{3}(3 - \sin\phi_r)}$$

, where

$\phi_{p,r}$  are peak and residual friction angle, respectively.

## 1. Constitutive models

### 1.2 Nonassociated Flow Rule (NA)

Since there may be a range of possible solutions, each associated with a different pattern of localization and all of which are entirely valid, it can be expected that any numerical solution will be very sensitive to both physical imperfections as well as round-off errors and the exact sequence in which the procedures defining the solution scheme are carried out. In the end, the result is a load-displacement response that tends to be rather oscillatory.

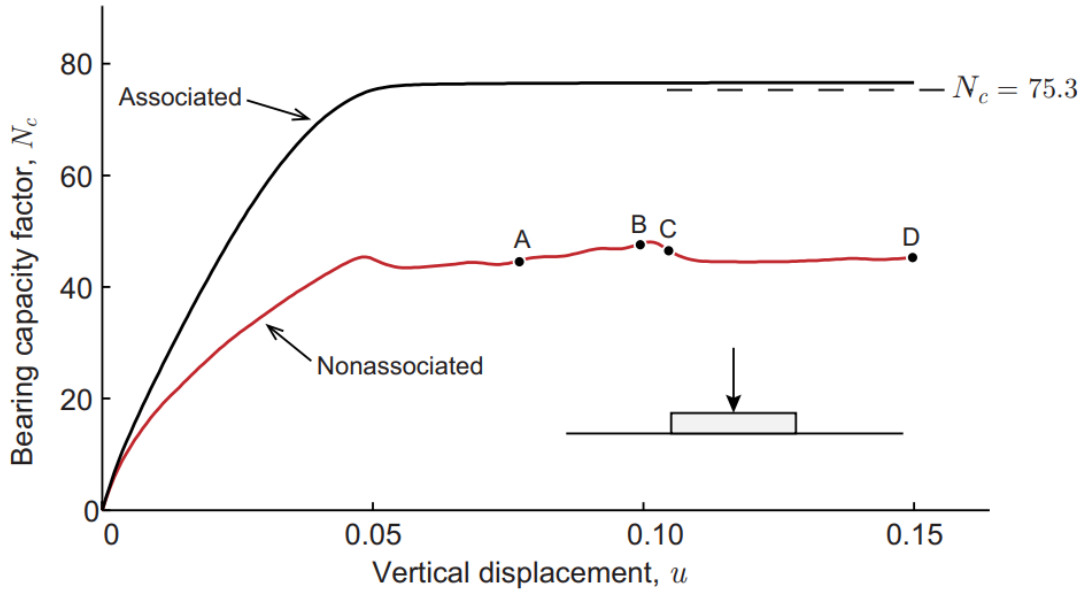


**Figure 1.1:** Load-displacement response for strip footing on a weightless soil (After Krabbenhoft et al., 2012)

The basic idea behind the formulation derives from the structure of the internal dissipation associated with constitutive models. Let us assume a yield function of the type:

$$F = Mp + q - c$$

, where

$p$  and  $q$  are mean and deviatoric stress,  $M$  is a friction coefficient, and  $c$  is cohesion.

## 1. Constitutive models

The plastic potential function is given by:

$$G = Np + q$$

, where  $N \leq M$  is a dilation coefficient.

In  $p - q$  triaxial space, the plastic strain rates are given by:

$$\delta\varepsilon_v^p = \delta\lambda \frac{\partial G}{\partial p} = \delta\lambda N \delta\varepsilon_s^p = \delta\lambda \frac{\partial G}{\partial p} = \delta\lambda$$

, where  $\delta$  denotes time increment,  $\varepsilon_v^p$  and  $\varepsilon_s^p$  are volumetric and deviatoric plastic strains conjugate to  $p$  and  $q$ , respectively.

The dissipation  $D$  is given by:

$$\begin{aligned} D &= p\varepsilon_v^p + q\varepsilon_s^p \\ &= (Nq + q)\delta\lambda \\ &= [c - (M - N)p]\delta\lambda \\ &= [c - (M - N)p]\varepsilon_s^p \end{aligned}$$

The above-mentioned parameters are all related with the confining pressure, which can be easily illustrated with the figure below:

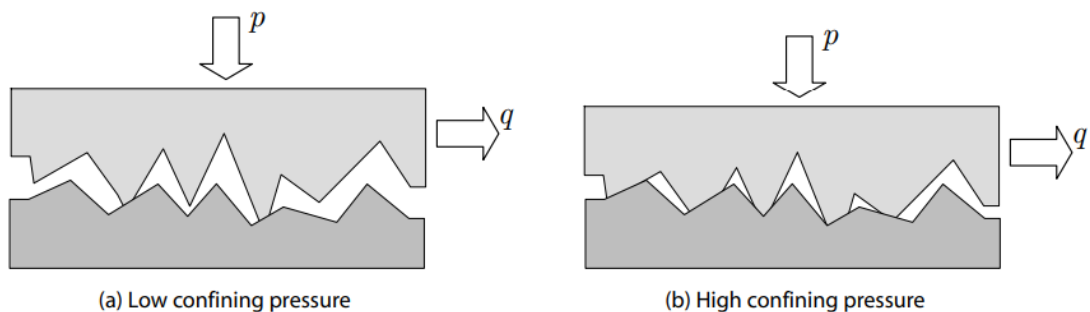


**Figure 1.2:** Microscopic origins of friction as plastic shearing of asperities. A higher confining pressure implies a higher degree of interlocking of the asperities and thereby a higher apparent shear strength (After Krabbenhoft et al., 2012)

## 1. Constitutive models

### 1.3 Extended Mohr—Coulomb Model (EMC)

The elastic-perfectly plastic Mohr-Coulomb model is widely used for geotechnical analysis. It provides very crude match to actual shearing behavior of soils. A natural extension is to create a hardening version of the M-C model in which the size of the yield surface varies in some nonlinear way with the development of plastic strain. In the model to be described as hardening will be linked only with distortional strain. It is useful for modelling sands , where it is rearrangement of the rather particles that dominates the response and irrecoverable volumetric changes are essentially linked by this rearrangement of particles (Wood, 2004).

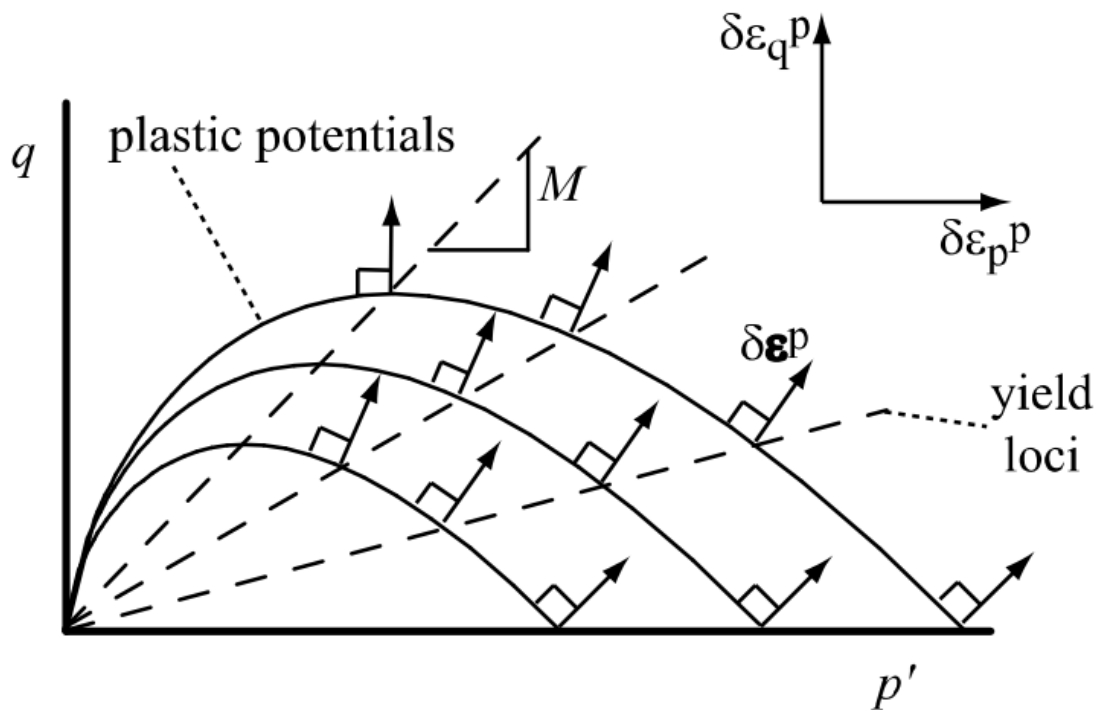


**Figure 1.3:** Plastic potential curves (solid lines) and yield loci (dashed lines) in elastic-hardening plastic Mohr-Coulomb model

Following Taylor's (1948) proposal of a link between dilatancy and mobilized friction in a shear box test, stress—dilatancy equation expressed in terms of total strain increments is obtained.

## 1. Constitutive models

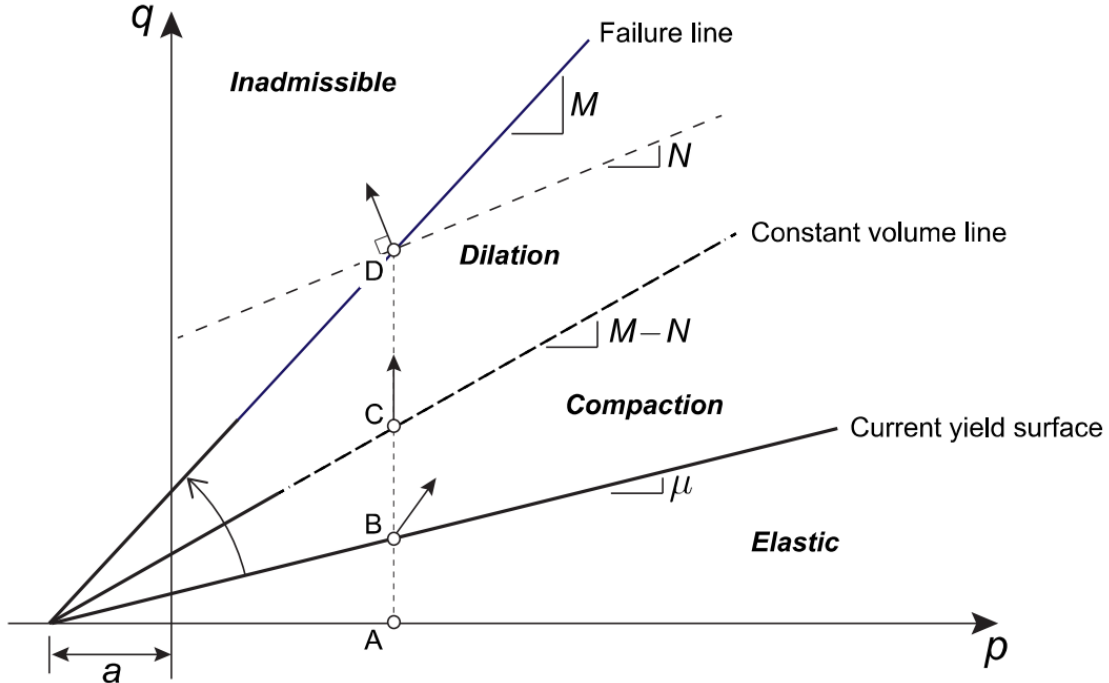


**Figure 1.4:** Hardening, compaction and dilation in the HMC model

### 1.3.1 Comparison between associated and non-associated flow rule in plastic model

In the elastic-perfectly-plastic Mohr-Coulomb model, it is commonly assumed that the plastic potential takes the same form as the yield surface, but with the slope defined by a dilation angle  $\psi$  rather than a friction angle. If this assumption is adopted, then the direction of the plastic strain increment  $\delta\varepsilon^p$  would be normal to a set of parallel lines by the dilation angle. If normality rule were assumed, radical difference between the slope of yield criterion line and the plastic potential contour is observed (J.P. Doherty and D. Muir Wood, 2013).

### 1. Constitutive models

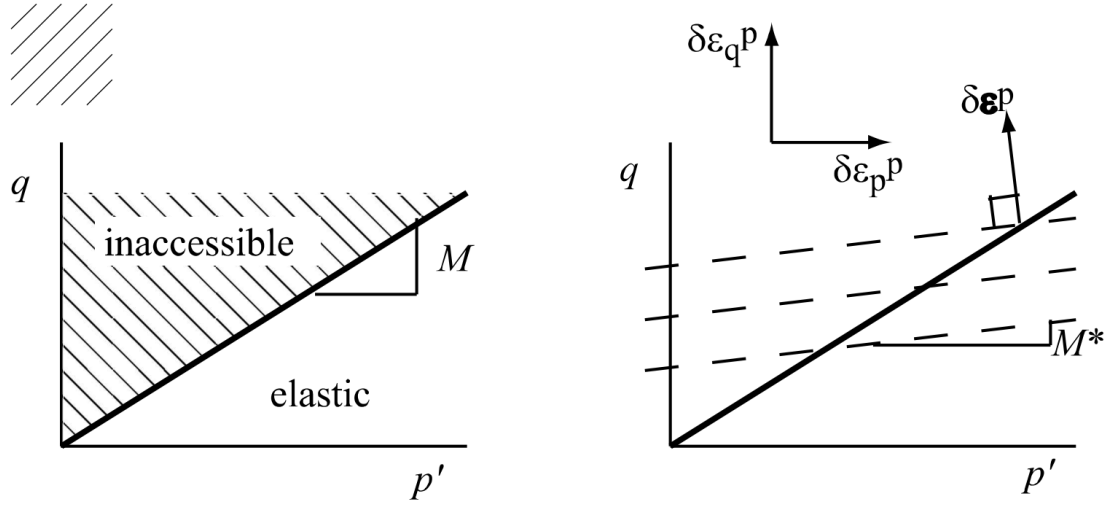


**Figure 1.5:** Elastic-perfectly plastic Mohr-Coulomb model (a) yield and failure locus, (b) plastic potentials

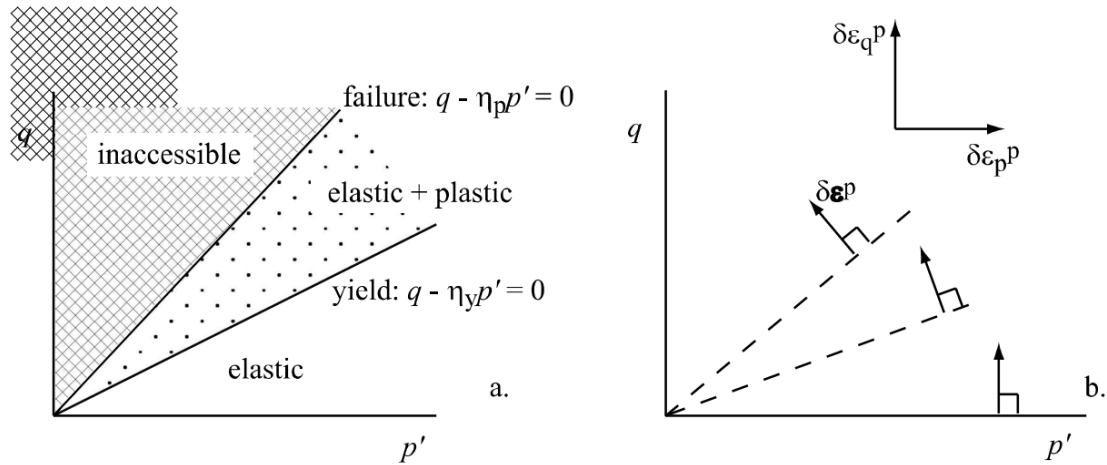


**Figure 1.6:** Elastic-hardening plastic Mohr-Coulomb model (a) yield locus and failure locus separating elastic plastic and inaccessible regions of stress plane (b) normality applied at the plastic region

### 1.3.2 Yield function

$$F(\vec{\sigma}, \chi) = F(p', q, \chi) = q - \eta_y p' = 0$$

### 1.3.3 Plastic potential function

$$G(\vec{\sigma}) = q - (M - M')p' \ln\left(\frac{p'_x}{p'}\right) = 0$$

## 1. Constitutive models

, where  $\eta_{y,p}$  is stress ratio at yield and peak, respectively,

$p'_r$  is chosen s.t. plastic potential gradient passes through current stress, i.e.,

$$p'_r = p' \exp\left\{\frac{\eta_y}{M-M'}\right\}$$

$M$  is material parameter at perfect plasticity when hardening terminates.

$$M = \frac{6\sin\phi}{3-\sin\phi}$$

$M'$  is dilation at constant volume line:

$$M' = \frac{6\sin\psi}{3-\sin\psi}$$

$$M' = M - k\psi = M - k(v - \Gamma + \lambda \ln p')$$

$k$  is soil constant linking state variable and strength.

Critical State description is as follows:

$$M' = M - k[(v_0 - \Gamma + \lambda \ln p'_0 + (\lambda \ln \frac{p'}{p'_0} - v_0 \varepsilon_p^e) - v_0 \varepsilon_p^p)].$$

### 1.3.4 Flow rule

$$\frac{\delta \varepsilon_p^p}{\delta \varepsilon_q^p} = M - M' - \eta_y$$

### 1.3.5 Hardening

$$\delta \eta_y = \frac{1 - \frac{\eta_y}{M}}{\beta} \delta \varepsilon_q^p$$

, where

$\beta$  is a model parameter scaling plastic strain,

$$\beta = \frac{3}{2} p' \frac{9-M}{9-(M-M')M \ln 2 - 3M'} \frac{1-E_{50}/E_{ur}}{E_{50}} \text{ for Taylor's } \sigma - \psi \text{ relation.}$$

The incremental of the stress ratio is defined as:

$$\delta \eta_y = \frac{3 \sin \delta \phi}{\sqrt{3} \cos \theta + \sin \theta \sin \delta \phi}$$

### 1.3.6 Soil Parameters

#### Elastic Moduli

The elastic moduli are estimated from the modified equation proposed by Hardin and Black (1968) in the case of sand:

## 1. Constitutive models

$$G = G_0 \frac{(2.17 - e)^2}{1 + e} \sqrt{p'} K = \frac{1 + \nu}{3(1 - 2\nu)} G$$

, where

$\nu$  is Poisson's ratio,

$e$  is void ratio,

$G_0$  is initial shear modulus.

### Peak friction angle

The peak friction angle of  $\phi_p$  is estimated from the empirical relations proposed by Bolton (1987):

$$I_r = D_r [5 - \ln(\frac{p'}{150})] - 1, \quad (p' \geq 150 kN/m^2) \\ I_r = 5D_r - 1, \quad (p' < 150 kN/m^2) \\ \phi_p = 3I_r + \phi_r$$

### Dilatancy angle

The dilatancy angle of  $\psi$  is estimated from modified Rowe's stress-dilatancy relationship:

$$\sin\psi = \frac{\sin\phi - \sin\phi'_r}{1 - \sin\phi \sin\phi'_r} \phi'_r = \phi_r [1 - \beta \exp\{-(\frac{\chi}{\epsilon_d})^2\}]$$

, where

$\beta$  and  $\epsilon_d$  are stress—dilatancy material parameters.

$E_{50}$  is a secant modulus defined as:

$$E_{50} = \frac{\frac{1}{2}q_u}{\epsilon_{a,50}}$$

$E_{ur}$  is unloading/reloading stiffness.

# 2

## Calibration and Validation

### Contents

---

|            |  |           |
|------------|--|-----------|
| <b>2.1</b> | <b>Drained Triaxial Test</b>               | <b>13</b> |
| <b>2.2</b> | <b>Soil Parameters</b>                     | <b>16</b> |
| 2.2.1      | Strain—Softening Stiffness—Hardening Model | 16        |
| 2.2.2      | Nonassociated Flow Rule (NA)               | 16        |
| 2.2.3      | Extended Mohr—Coulomb Model (EMC)          | 17        |
| <b>2.3</b> | <b>Convergence Criteria</b>                | <b>18</b> |
| 2.3.1      | Mesh Convergence                           | 18        |
| 2.3.2      | Boundary Convergence                       | 25        |

---

For the validity of the finite element tests performed, the triaxial elemental test is simulated with the box of union length. The set up is as follows:

2. Calibration

## 2.1 Drained Triaxial Test

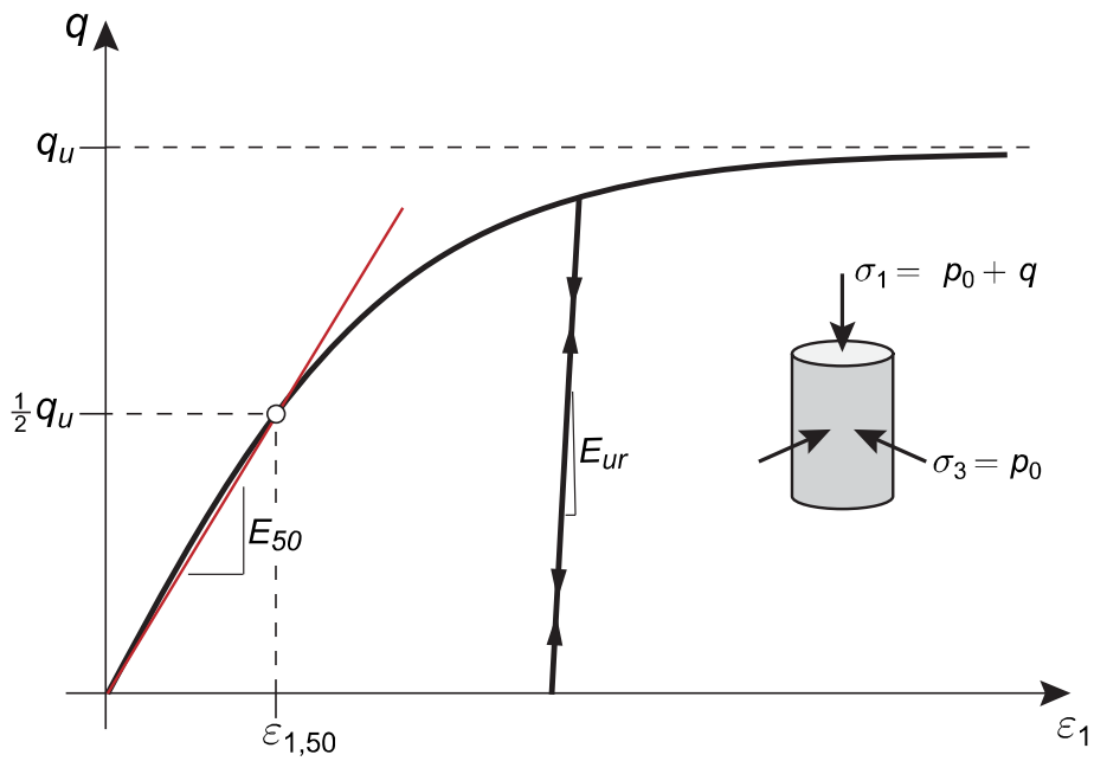


**Figure 2.1:** Typical triaxial test (After Krabbenhoft, 2013)

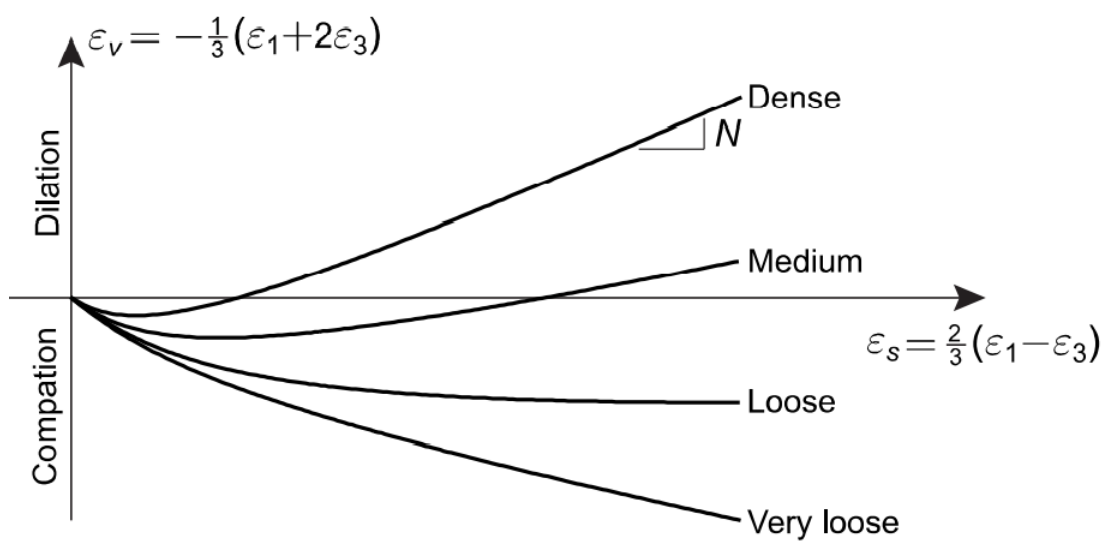


**Figure 2.2:** Typical shear-volumetric strain behavior in triaxial compression (After Krabbenhoft, 2013)

## 2. Calibration

Two tests — Triaxial compression and extension (TC/TE) — are simulated using Multiplier Elasto—plastic analysis under axisymmetric conditions as indicated in the Figure below. The fixed loads here represent the initial axial and radial stresses while the axial Multiplier load is increased in the course of the analysis to reach the ultimate limit state.

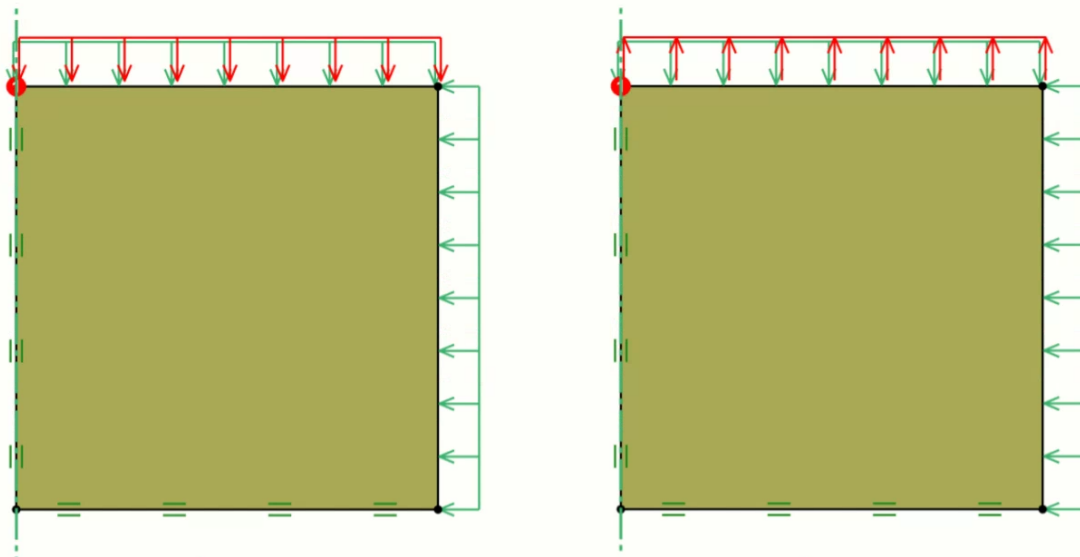


**Figure 2.3:** Setup for elemental triaxial compression and extension

By a process of trial and error, the fits shown in Figure are obtained. For this data set , where no information about the behavior in simple shear is available the value is well within range that can be accommodated by the isotropic strength option, there is little reason to assume any anisotropy. We note that the compression secant modulus in compression is only half of the extension secant modulus. This is somewhat unusual, but in this case nevertheless what fits the data best.

### Result of Elemental Triaxial Test at 100 kPa

Triaxial test at radial stress of 100 kPa is simulated using one by one block of the finite element formulation with the EMC model.

## 2. Calibration

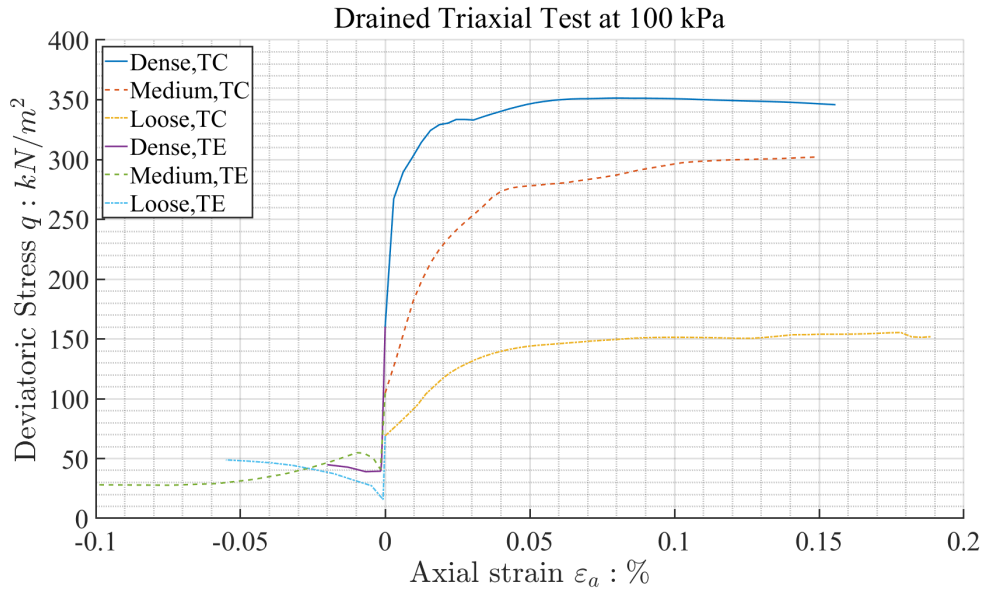


**Figure 2.4:** Result of Drained Triaxial test at 100 kPa

## Result of Elemental Triaxial Test at 200 kPa

Triaxial test at radial stress of 200 kPa is simulated using one by one block of the finite element formulation with the EMC model.

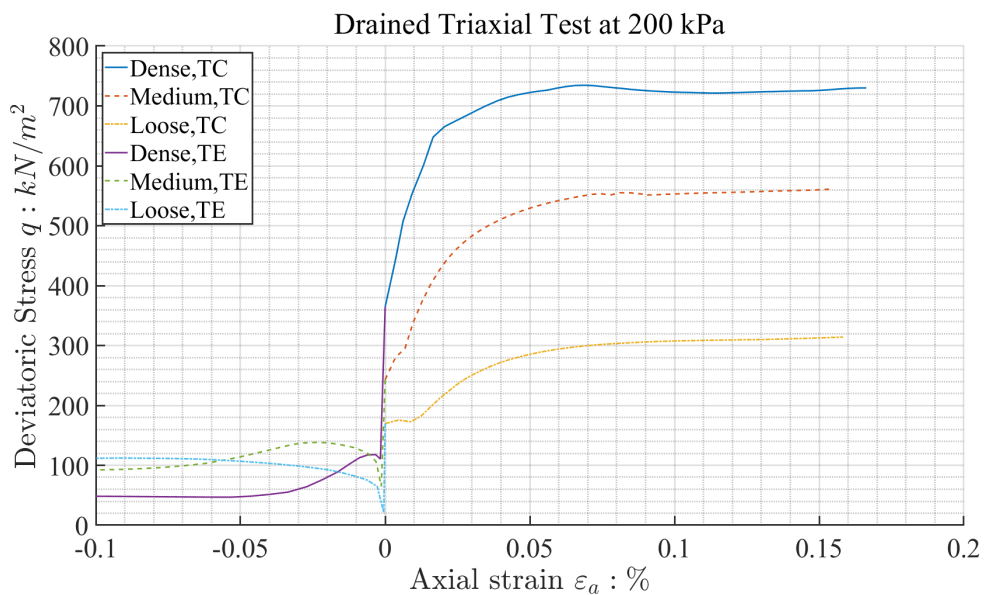


**Figure 2.5:** Result of Drained Triaxial test at 200 kPa

2. Calibration

## 2.2 Soil Parameters

### 2.2.1 Strain—Softening Stiffness—Hardening Model

Here is a table presenting the model parameters used by Sakai and Tanaka (1993).

| Parameters                                  | Loose | Medium | Dense |
|---|-------|--------|-------|
| Density $\gamma(kN/m^3)$                    | 13.5  | 14.8   | 16.3  |
| Void ratio $e$                              | 0.95  | 0.78   | 0.62  |
| Relative density $D_r$                      | 0.05  | 0.53   | 0.95  |
| Coefficient of shear modulus, $G_0$         | 500   | 500    | 500   |
| Poisson's ratio, $\nu$                      | 0.3   | 0.3    | 0.3   |
| Peak friction angle, $\phi_p(^{\circ})$     | 33    | 38     | 45    |
| Residual friction angle, $\phi_r(^{\circ})$ | 33    | 33     | 33    |
| Dilation angle, $\psi(^{\circ})$            | 0     | 10     | 20    |
| Shear band thickness, $S.B.(cm)$            | 0.3   | 0.3    | 0.3   |
| Soil parameter, $a$                         | 0.1   | 0.1    | 0.1   |
| Soil parameter, $b$                         | 0.8   | 0.4    | 0.1   |
| Soil parameter, $\varepsilon_d$             | 0.3   | 0.3    | 0.3   |
| Soil parameter, $m$                         | 0.4   | 0.2    | 0.1   |
| Soil parameter, $\beta$                     | 0.1   | 0.1    | 0.1   |

**Table 2.1:** Model parameters used by Sakai and Tanaka, 1993

### 2.2.2 Nonassociated Flow Rule (NA)

Here is a table presenting the model parameters used in Nonassociated (NA) simulations.

## 2. Calibration

| Parameter              | Dense  | Medium | Loose |
|------------------------|--------|--------|-------|
| $E(MPa)$               | 50     | 25     | 15    |
| $\nu$                  | 0.3    | 0.25   | 0.2   |
| $c(kPa)$               | 0      | 0      | 0     |
| $\phi(^{\circ})$       | 40     | 35     | 30    |
| $\psi(^{\circ})$       | 10     | 5      | 0     |
| $\gamma_{dry}(kN/m^3)$ | 18     | 16     | 14    |
| $\gamma_{sat}(kN/m^3)$ | 21     | 20     | 19    |
| $K_0$                  | 0.3572 | 0.4264 | 0.5   |

**Table 2.2:** Soil parameters used in nonassociated flow (NA) simulations

### 2.2.3 Extended Mohr—Coulomb Model (EMC)

Here is a table presenting the model parameters used in Extended Mohr-Coulomb (EMC) simulations.

| Parameter              | Dense  | Medium | Loose |
|------------------------|--------|--------|-------|
| $E_{50}(MPa)$          | 50     | 25     | 13    |
| $E_{ur}(MPa)$          | 150    | 75     | 39    |
| $\nu_{ur}$             | 0.4    | 0.35   | 0.3   |
| $c(kPa)$               | 0      | 0      | 0     |
| $\phi(^{\circ})$       | 41     | 37     | 27    |
| $\psi(^{\circ})$       | 17     | 11     | -4    |
| $\gamma_{dry}(kN/m^3)$ | 18     | 16     | 14    |
| $\gamma_{sat}(kN/m^3)$ | 21     | 20     | 19    |
| $K_0$                  | 0.3572 | 0.4264 | 0.5   |
| $p_{ref}(kPa)$         | 100    | 100    | 100   |
| Soil parameter, m      | 0.5    | 0.5    | 0.5   |

**Table 2.3:** Soil parameters used in Extended Mohr-Coulomb Model (EMC) simulations

## 2. Calibration

### 2.3 Convergence Criteria

#### 2.3.1 Mesh Convergence

Here is a table presenting the result of mesh convergence test on both NA and EMC models.

The goal of the mesh convergence test usually is to seek the acceptable range of number of the mesh size. However, the interest in the present paper differs from the previously investigated objectives, in a way that the object sought is not the same. The present paper seeks to draw a more detailed analysis of the failure surface formed as the soil is sheared.

Some authors in the past described this with the width of the shear band (Tanaka and Sakai, 1993). However, the present paper deals only with the limit analysis formulation using the Extended Mohr-Coulomb model.

| Type of Analysis           | Mesh Number | $p_u, kN/m^2$ | Variance | Std  |
|----------------------------|-------------|---------------|----------|------|
| Non-associated (NA)        | 250         | 137.7         | 0.11     | 0.33 |
| Non-associated (NA)        | 500         | 135.8         | 1.23     | 1.11 |
| Non-associated (NA)        | 1000        | 129.4         | 13.85    | 3.72 |
| Non-associated (NA)        | 2000        | 139.8         | 0.28     | 0.52 |
| Non-associated (NA)        | 5000        | 138.2         | 0.02     | 0.13 |
| Non-associated (NA)        | 10000       | 141.7         | 1.69     | 1.30 |
| Non-associated (NA)        | 20000       | 147           | 12.00    | 3.46 |
| Exteded Mohr-Coulomb (EMC) | 250         | 161.3         | 1.51     | 1.23 |
| Exteded Mohr-Coulomb (EMC) | 500         | 159.6         | 0.29     | 0.54 |
| Exteded Mohr-Coulomb (EMC) | 1000        | 161.4         | 1.62     | 1.27 |
| Exteded Mohr-Coulomb (EMC) | 2000        | 158.4         | 0.00     | 0.05 |
| Exteded Mohr-Coulomb (EMC) | 5000        | 157.3         | 0.16     | 0.40 |
| Exteded Mohr-Coulomb (EMC) | 10000       | 156.2         | 0.73     | 0.85 |
| Exteded Mohr-Coulomb (EMC) | 20000       | 153.8         | 3.35     | 1.83 |

**Table 2.4:** Setup and result of mesh convergence test

## 2. Calibration

### Mesh Convergence Results

The result of the present investigation is the determination of the number of the mesh elements be around 2000.

However, it is noted that further studies, outside of this paper, is onto the maximum number of the elements to be studied, for this will enhance the visualization of the shear band formation, as well as the guidance onto the study of the shear dissipation.

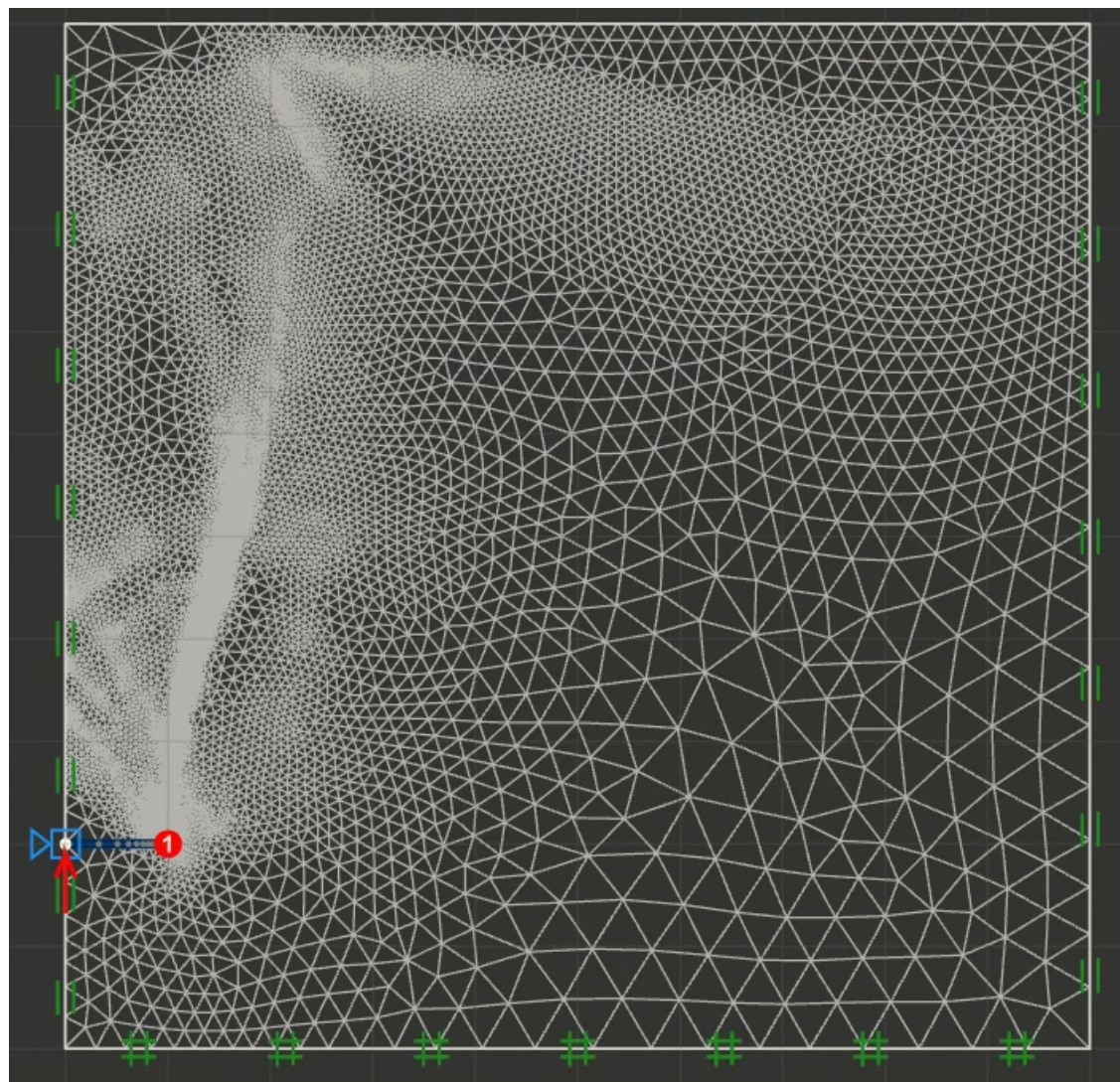


**Figure 2.6:** Typical result from mesh convergence test (maximum number of elements)

## 2. Calibration

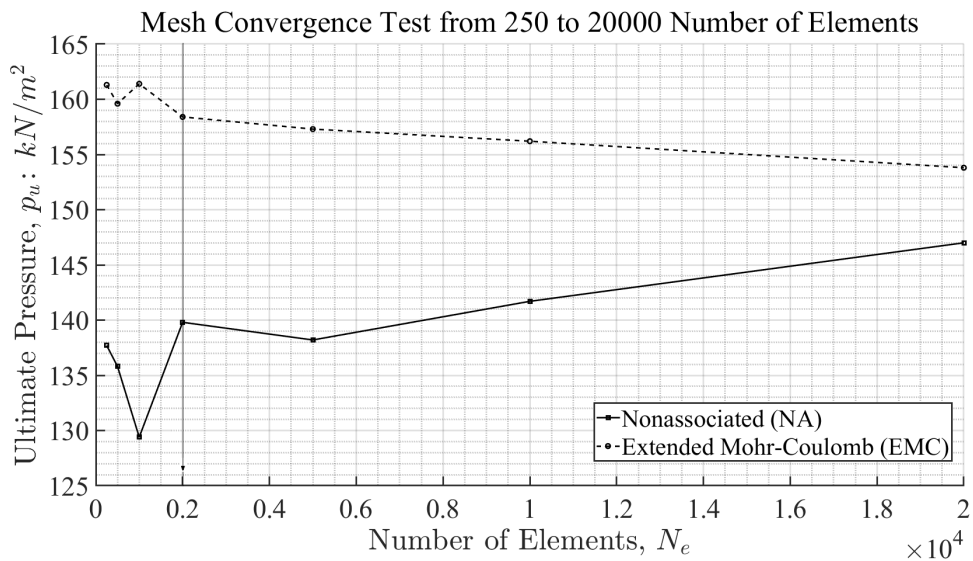


**Figure 2.7:** Result of the mesh convergence test, which confirms that about 2000 elements are acceptable

## 2. Calibration

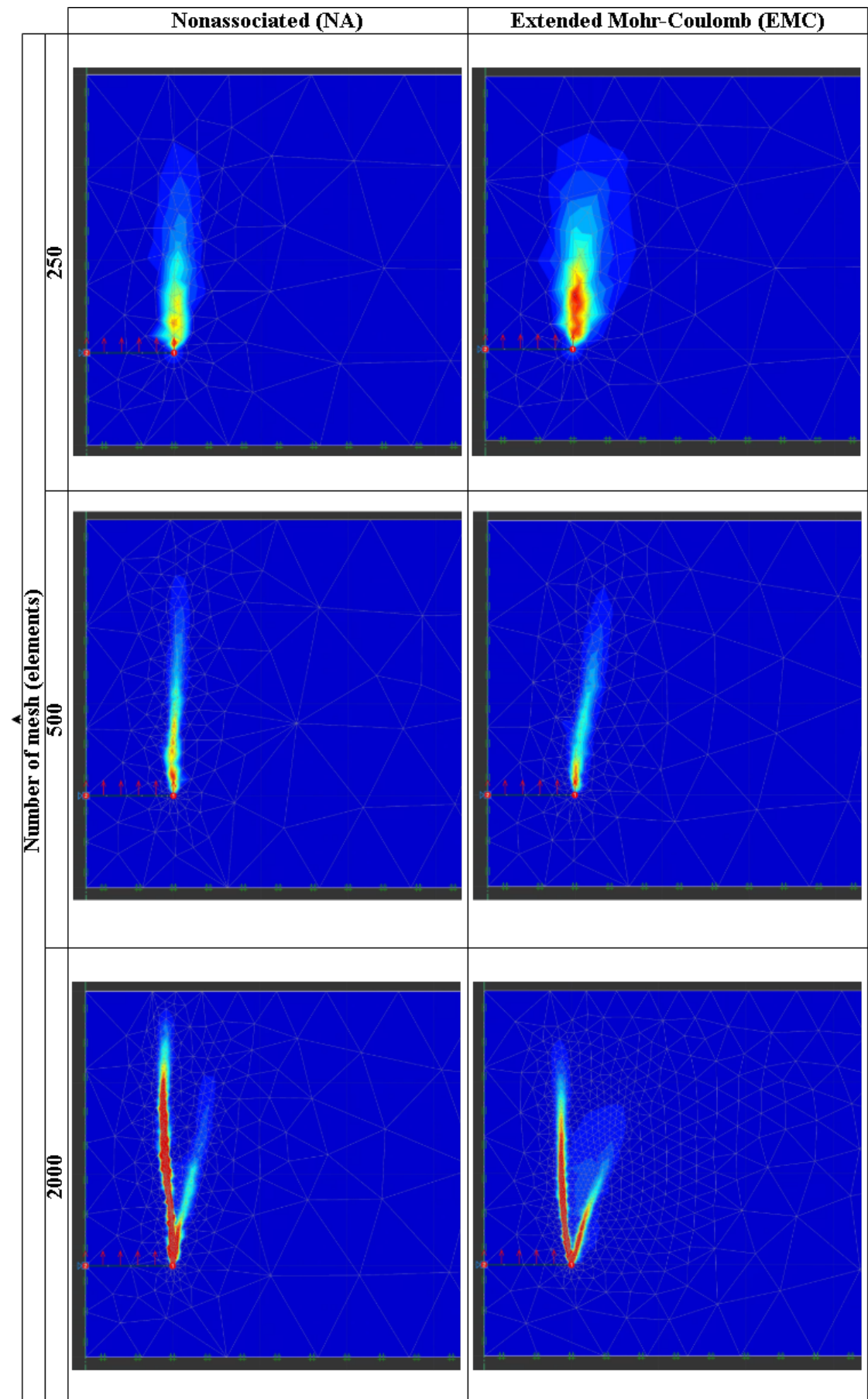
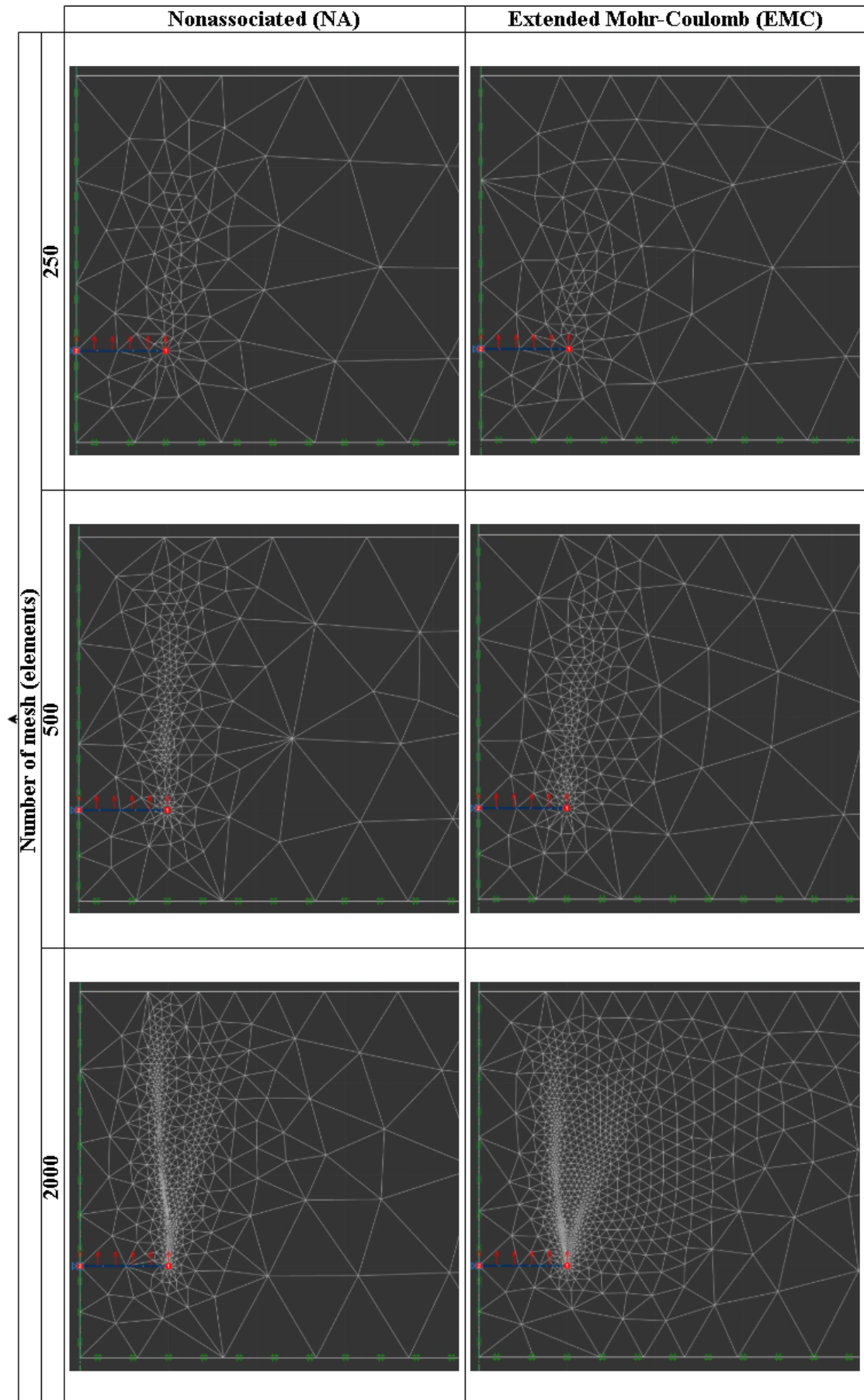


Figure 2.8: Shear Dissipation of the mesh convergence test of 250, 500, 2000 elements <sup>21</sup>

## 2. Calibration



**Figure 2.9:** Mesh of 250, 500, 2000 elements

## 2. Calibration

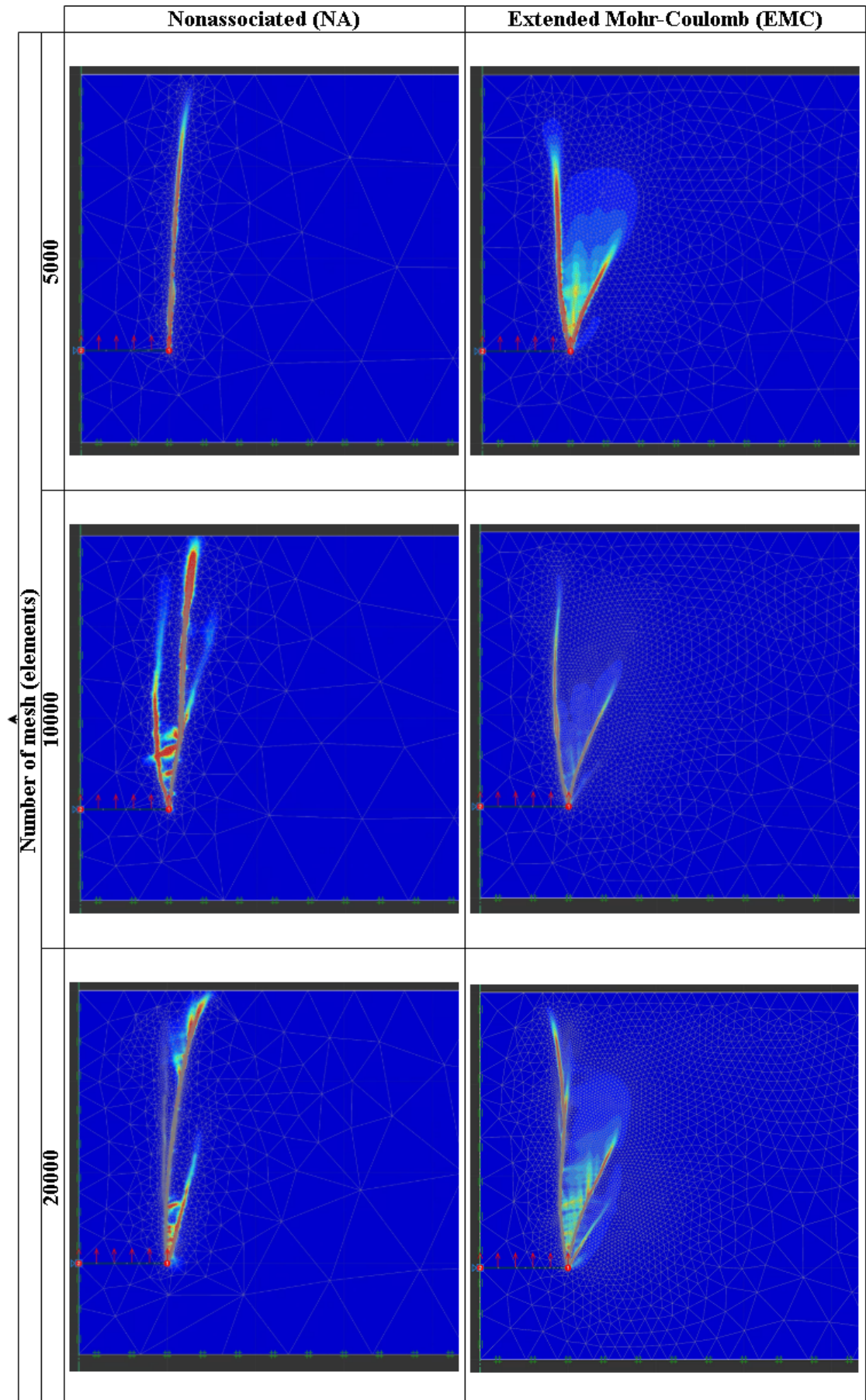


**Figure 2.10:** Shear Dissipation of the mesh convergence test of 5000, 10000, 20000<sup>23</sup> elements

## 2. Calibration

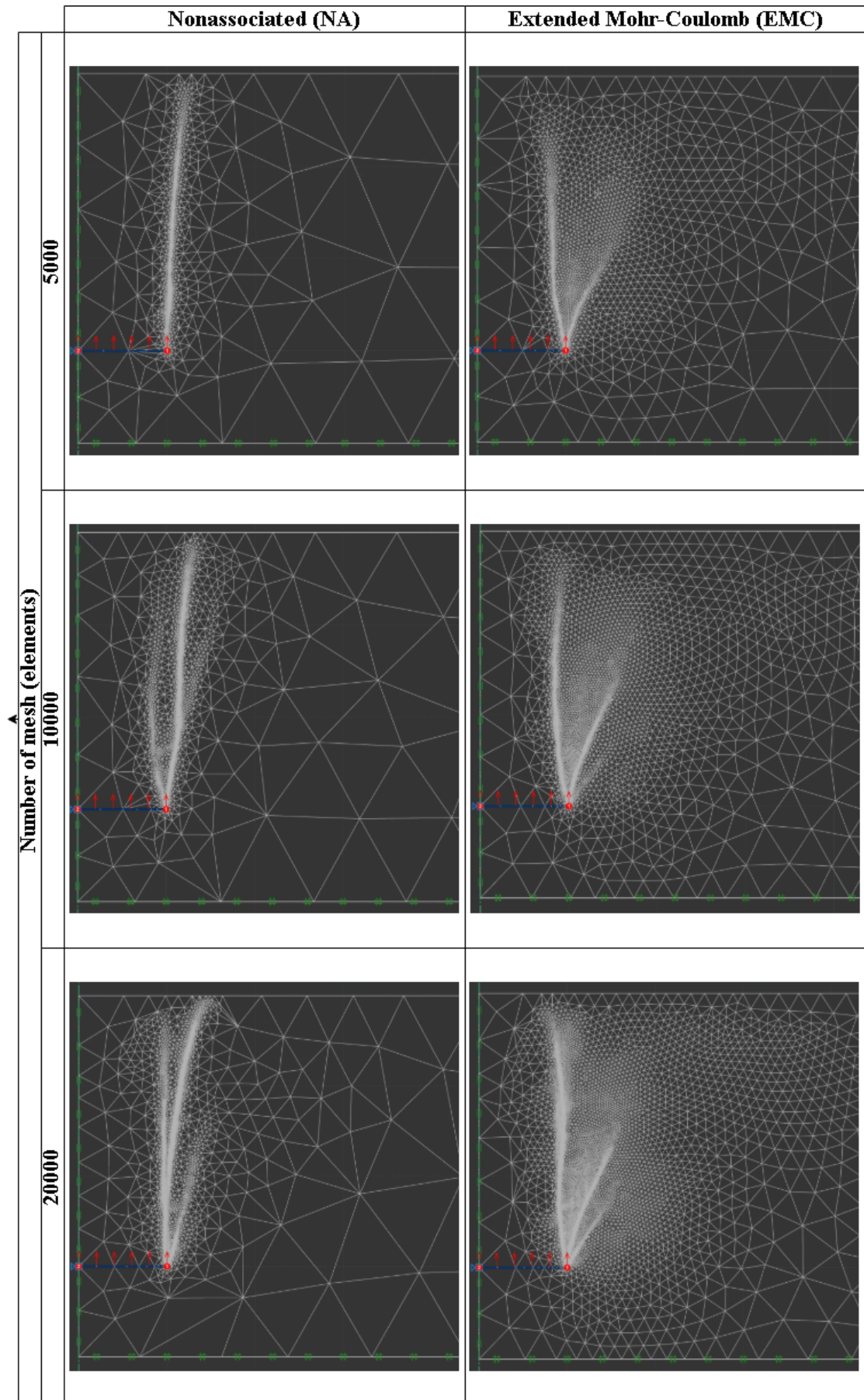


**Figure 2.11:** Mesh of 5000, 10000, 20000 elements

## 2. Calibration

### 2.3.2 Boundary Convergence

The soil tank width and the distance below the anchor to the soil tank boundary

are the primary concern for the modeling.

Therefore, the optimized value of the soil tank width has been investigated, by differing the values from 10B to 3B, , wherein B refers to the width of the anchor plate.

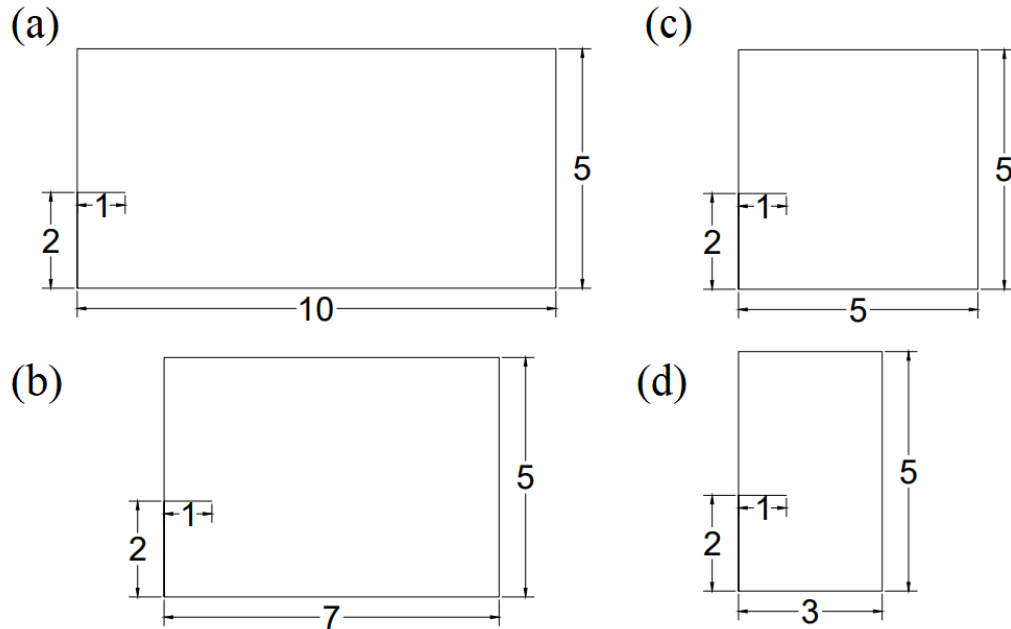


**Figure 2.12:** Convergence test setup on different boundary size: (a) 10B, (b) 7B, (c) 5B, (d) 3B

Due to the reasoning which considers the method of mesh adaptivity, insignificant effect onto the extension of the soil tank width has been deemed acceptable by the author. Therefore, the result of the boundary convergence test is determined at 10B.

## 2. Calibration

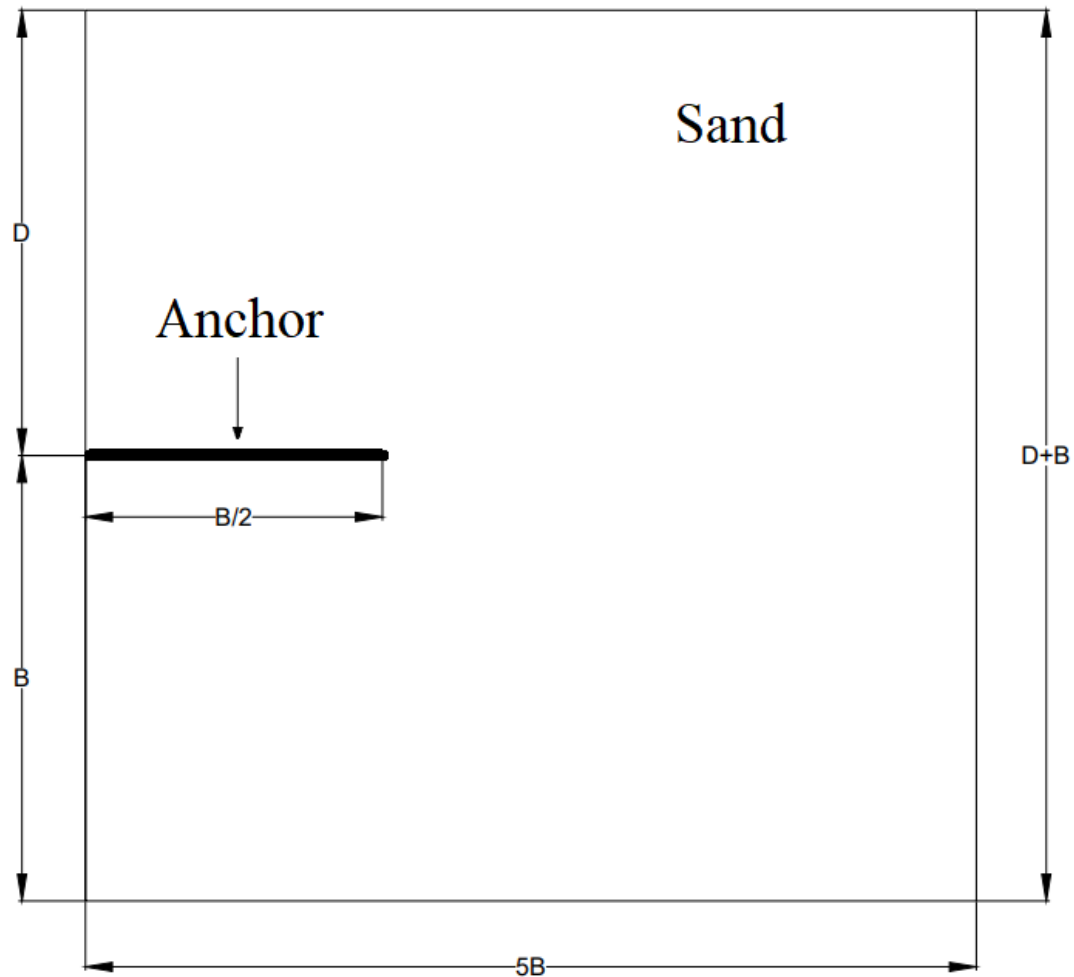


**Figure 2.13:** Final boundary decision schematic for numerical simulations

Here is a table presenting the setup of boundary convergence test on both NA and EMC models.

*2. Calibration*

| Width Boundary | Depth Below Anchor | D/B | Soil Type | Test Type |
|----------------|--------------------|-----|-----------|-----------|
| 10B            | 2B                 | 3   | Dense     | NA, EMC   |
| 7B             | 2B                 | 3   | Dense     | NA, EMC   |
| 5B             | 2B                 | 3   | Dense     | NA, EMC   |
| 3B             | 2B                 | 3   | Dense     | NA, EMC   |
| 10B            | 2B                 | 3   | Medium    | NA, EMC   |
| 7B             | 2B                 | 3   | Medium    | NA, EMC   |
| 5B             | 2B                 | 3   | Medium    | NA, EMC   |
| 3B             | 2B                 | 3   | Medium    | NA, EMC   |
| 10B            | 2B                 | 3   | Loose     | NA, EMC   |
| 7B             | 2B                 | 3   | Loose     | NA, EMC   |
| 5B             | 2B                 | 3   | Loose     | NA, EMC   |
| 3B             | 2B                 | 3   | Loose     | NA, EMC   |

**Table 2.5:** Setup of boundary convergence test

**Boundary Convergence Results**

# 3

## Results

### Contents

---

|   |           |
|---|-----------|
| <b>3.1 Parametric Study</b> . . . . .                         | <b>28</b> |
| 3.1.1 Effect of Embedment Depth Ratio $\frac{D}{B}$ . . . . . | 31        |
| 3.1.2 Effect of Width $B$ . . . . .                           | 32        |
| 3.1.3 Shear Dissipation . . . . .                             | 32        |
| <b>3.2 Comparison with Previous Researchers</b> . . . . .     | <b>39</b> |

---

### 3.1 Parametric Study

Here is a table presenting the setup of the numerical simulations on both NA and EMC models.

The code refers to the differing width of the plate anchor, , whereas the number specifies if its embedment ratio is either 1, 2, or 3.

### 3. Result

**Table 3.1:** Setup for numerical simulations

| Code | Test No. | Density | B, mm | D, mm | D/B |
|------|----------|---------|-------|-------|-----|
| A    | LA1      | Loose   | 40    | 40    | 1   |
| B    | LB1      | Loose   | 200   | 200   | 1   |
| C    | LC1      | Loose   | 1000  | 1000  | 1   |
| D    | LD1      | Loose   | 3500  | 3500  | 1   |
| E    | LE1      | Loose   | 4500  | 4500  | 1   |
| G    | LG1      | Loose   | 6500  | 6500  | 1   |
| A    | MA1      | Medium  | 40    | 40    | 1   |
| B    | MB1      | Medium  | 200   | 200   | 1   |
| C    | MC1      | Medium  | 1000  | 1000  | 1   |
| D    | MD1      | Medium  | 3500  | 3500  | 1   |
| E    | ME1      | Medium  | 4500  | 4500  | 1   |
| G    | MG1      | Medium  | 6500  | 6500  | 1   |
| A    | DA1      | Dense   | 40    | 40    | 1   |
| B    | DB1      | Dense   | 200   | 200   | 1   |
| C    | DC1      | Dense   | 1000  | 1000  | 1   |
| D    | DD1      | Dense   | 3500  | 3500  | 1   |
| E    | DE1      | Dense   | 4500  | 4500  | 1   |
| G    | DG1      | Dense   | 6500  | 6500  | 1   |
| A    | LA2      | Loose   | 40    | 80    | 2   |
| B    | LB2      | Loose   | 200   | 400   | 2   |
| C    | LC2      | Loose   | 1000  | 2000  | 2   |
| D    | LD2      | Loose   | 3500  | 7000  | 2   |
| E    | LE2      | Loose   | 4500  | 9000  | 2   |
| G    | LG2      | Loose   | 6500  | 13000 | 2   |
| A    | MA2      | Medium  | 40    | 80    | 2   |
| B    | MB2      | Medium  | 200   | 400   | 2   |
| C    | MC2      | Medium  | 1000  | 2000  | 2   |
| D    | MD2      | Medium  | 3500  | 7000  | 2   |
| E    | ME2      | Medium  | 4500  | 9000  | 2   |
| G    | MG2      | Medium  | 6500  | 13000 | 2   |

*3. Result*

**Table 3.1 continued from previous page**

| Code | Test No. | Density | B, mm | D, mm | D/B |
|------|----------|---------|-------|-------|-----|
| A    | DA2      | Dense   | 40    | 80    | 2   |
| B    | DB2      | Dense   | 200   | 400   | 2   |
| C    | DC2      | Dense   | 1000  | 2000  | 2   |
| D    | DD2      | Dense   | 3500  | 7000  | 2   |
| E    | DE2      | Dense   | 4500  | 9000  | 2   |
| G    | DG2      | Dense   | 6500  | 13000 | 2   |
| A    | LA3      | Loose   | 40    | 120   | 3   |
| B    | LB3      | Loose   | 200   | 600   | 3   |
| C    | LC3      | Loose   | 1000  | 3000  | 3   |
| D    | LD3      | Loose   | 3500  | 10500 | 3   |
| E    | LE3      | Loose   | 4500  | 13500 | 3   |
| G    | LG3      | Loose   | 6500  | 19500 | 3   |
| A    | MA3      | Medium  | 40    | 120   | 3   |
| B    | MB3      | Medium  | 200   | 600   | 3   |
| C    | MC3      | Medium  | 1000  | 3000  | 3   |
| D    | MD3      | Medium  | 3500  | 10500 | 3   |
| E    | ME3      | Medium  | 4500  | 13500 | 3   |
| G    | MG3      | Medium  | 6500  | 19500 | 3   |
| A    | DA3      | Dense   | 40    | 120   | 3   |
| B    | DB3      | Dense   | 200   | 600   | 3   |
| C    | DC3      | Dense   | 1000  | 3000  | 3   |
| D    | DD3      | Dense   | 3500  | 10500 | 3   |
| E    | DE3      | Dense   | 4500  | 13500 | 3   |
| G    | DG3      | Dense   | 6500  | 19500 | 3   |

### 3. Result

#### 3.1.1 Effect of Embedment Depth Ratio $\frac{D}{B}$

Overall Results with All Range of Dense, Medium, Loose Sands

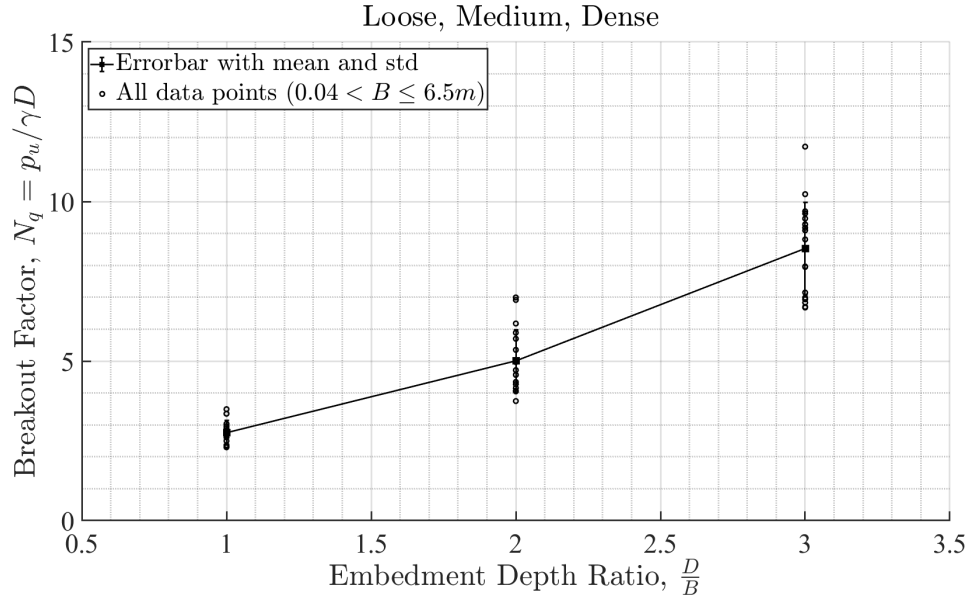


**Figure 3.1:** Effect of embedment depth ratio on break-out factor for all densities of soil

For Different Sand Densities: *Loose, Medium, Dense*

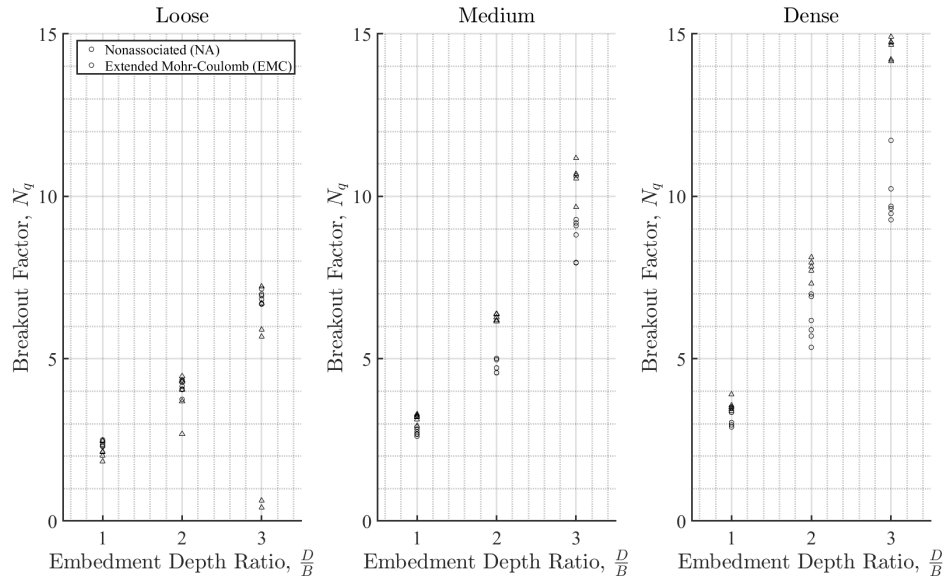


**Figure 3.2:** Effect of embedment depth ratio on break-out factor (a) loose (b) medium (c) dense

### 3. Result

#### 3.1.2 Effect of Width $B$

**Overall Results with All Range of Dense, Medium, Loose Sands**

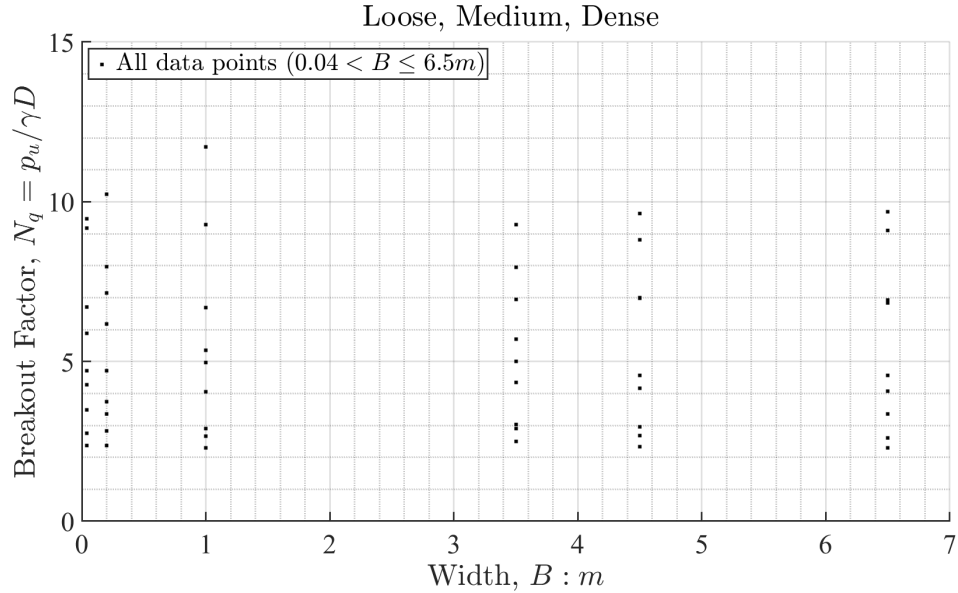


**Figure 3.3:** Effect of width of plate for all densities of soil

#### 3.1.3 Shear Dissipation

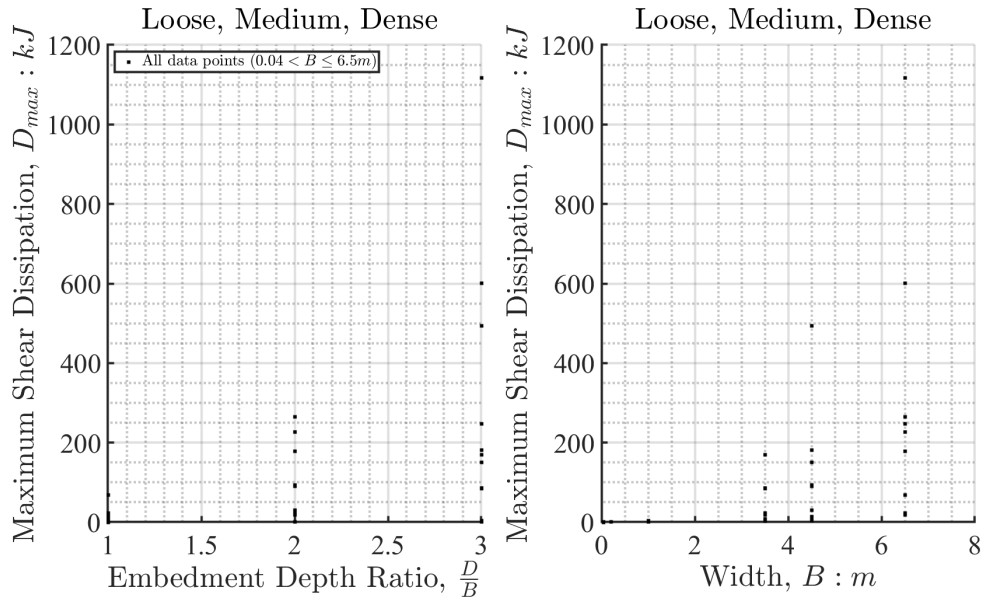


**Figure 3.4:** Effect of embedment depth and width on shear dissipation for all densities of soil

### 3. Result

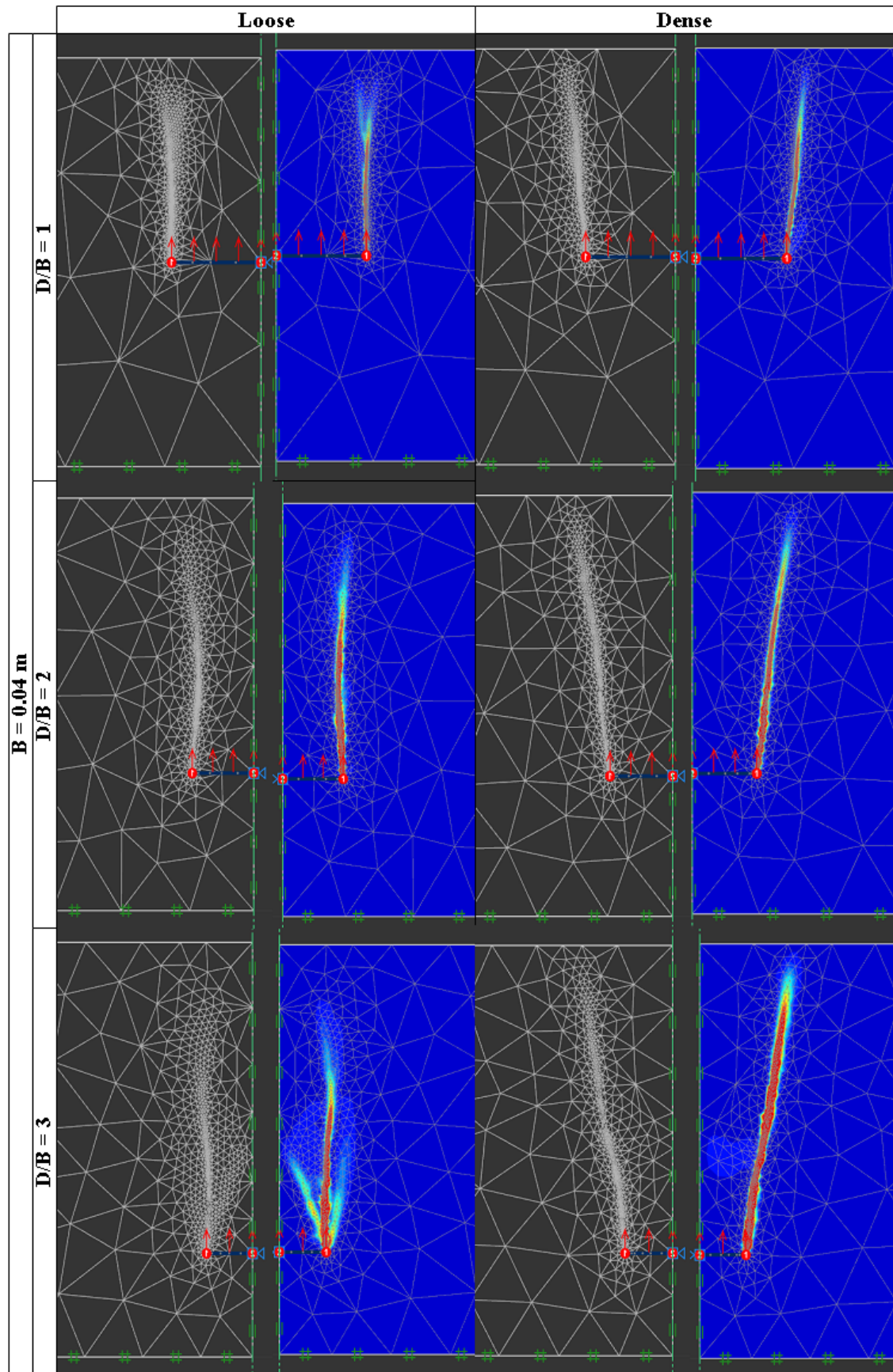


**Figure 3.5:** Shear dissipation of NA model at 10 percent of the maximum value and  $B = 0.04m$

### 3. Result

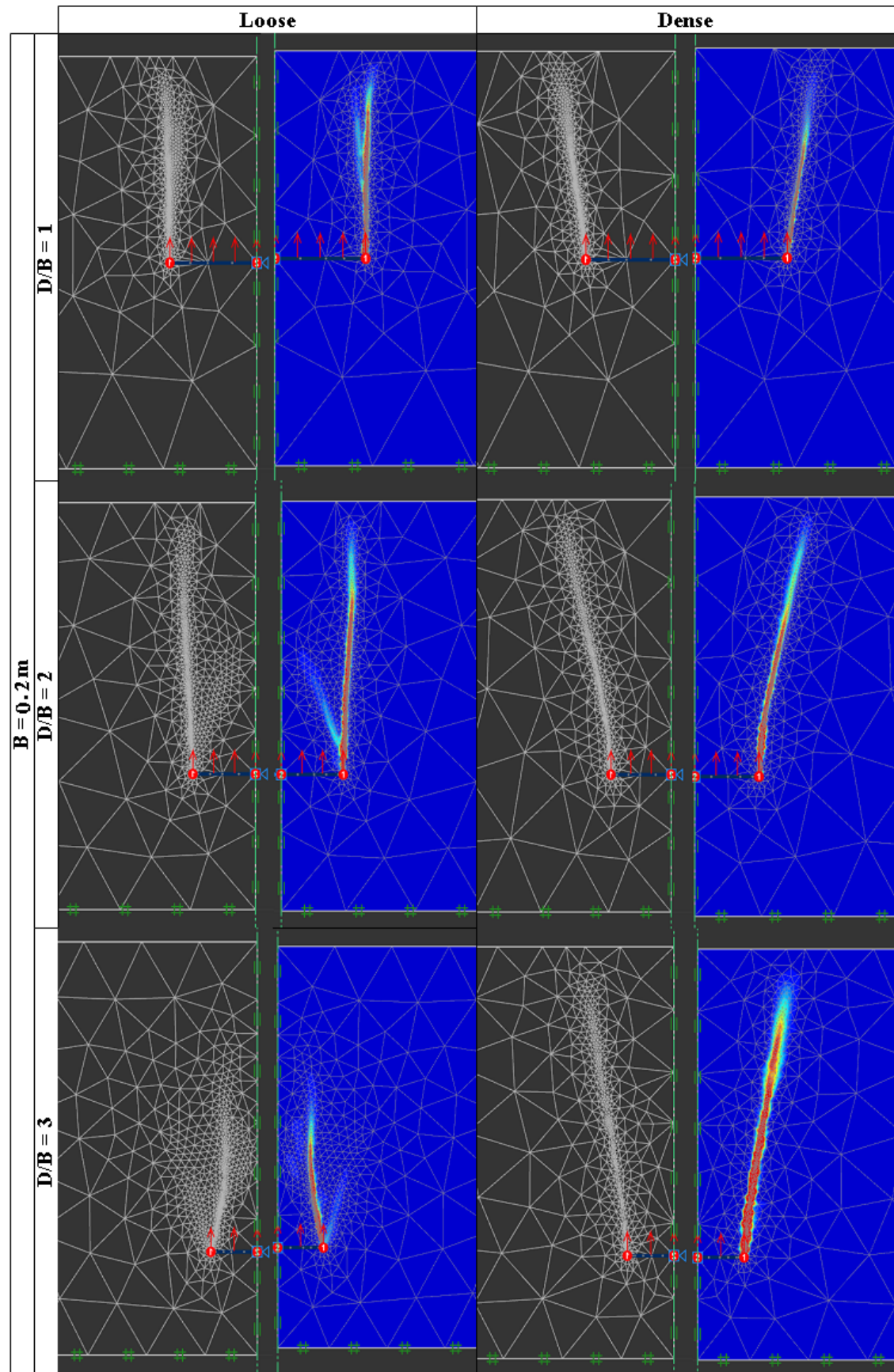


**Figure 3.6:** Shear dissipation of NA model at 10 percent of the maximum value and  $B = 0.2m$

### 3. Result

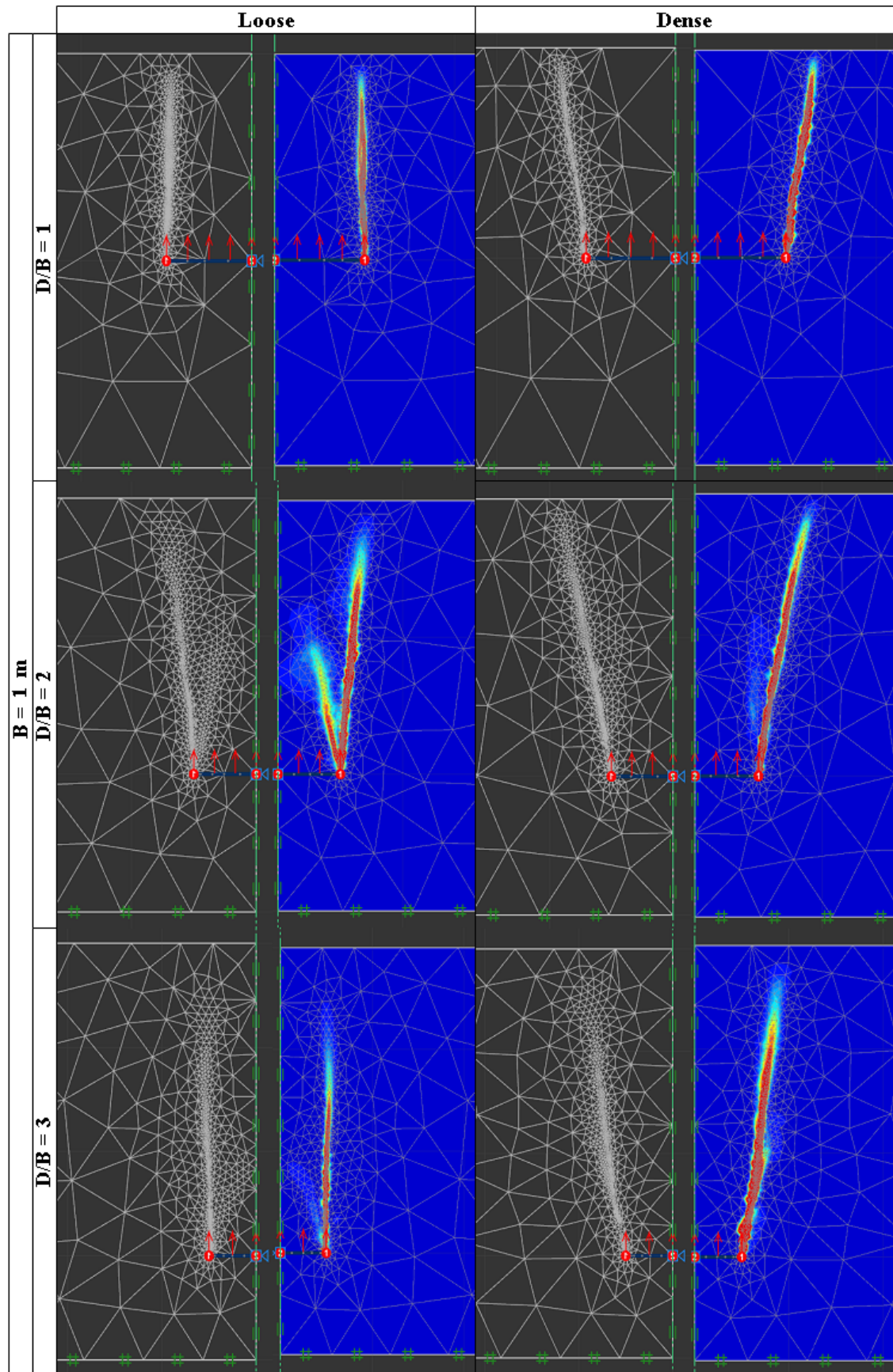


**Figure 3.7:** Shear dissipation of NA model at 10 percent of the maximum value and  $B = 1.0m$

### 3. Result

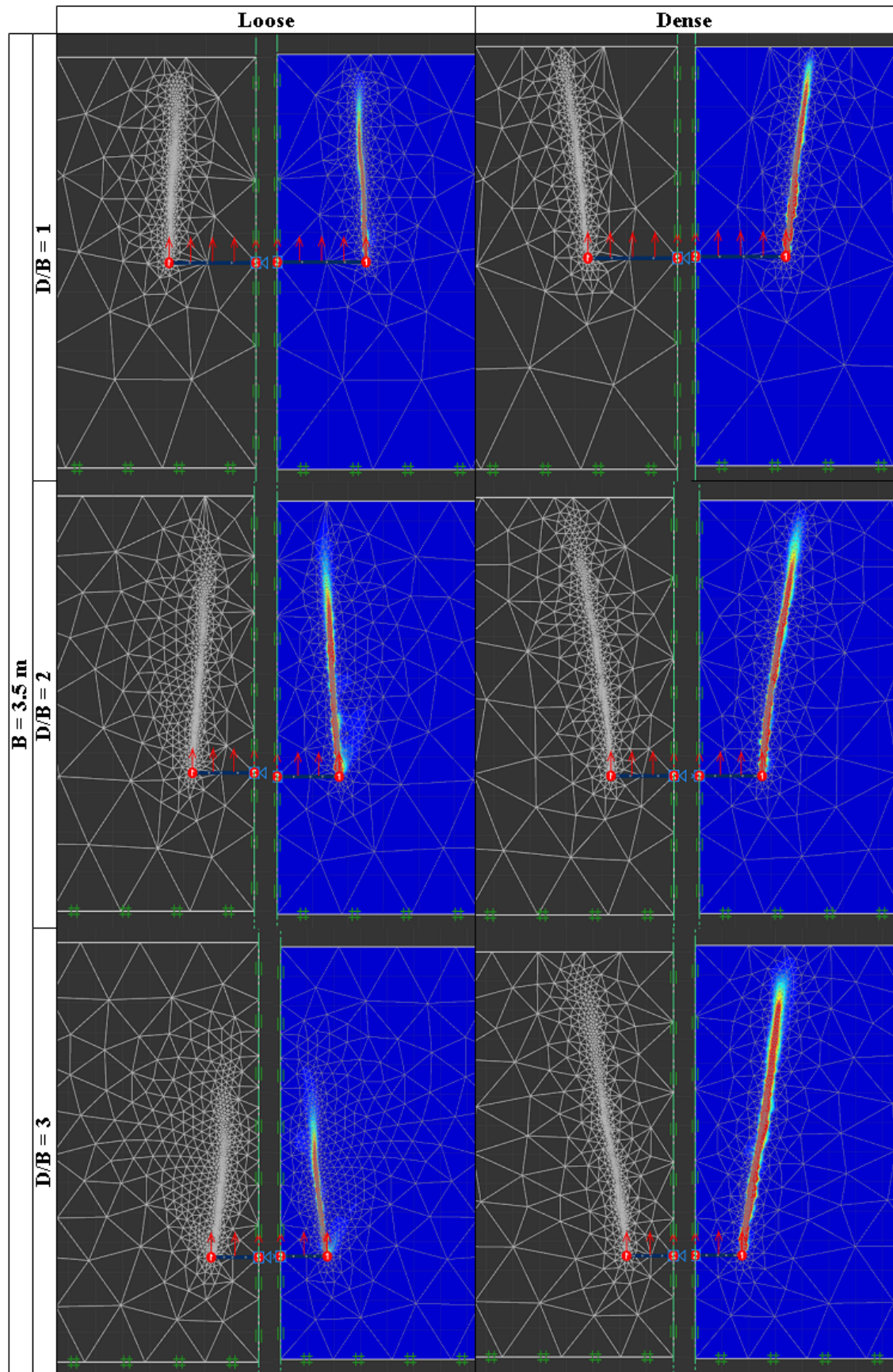


**Figure 3.8:** Shear dissipation of NA model at 10 percent of the maximum value and  $B = 3.5\text{m}$

### 3. Result

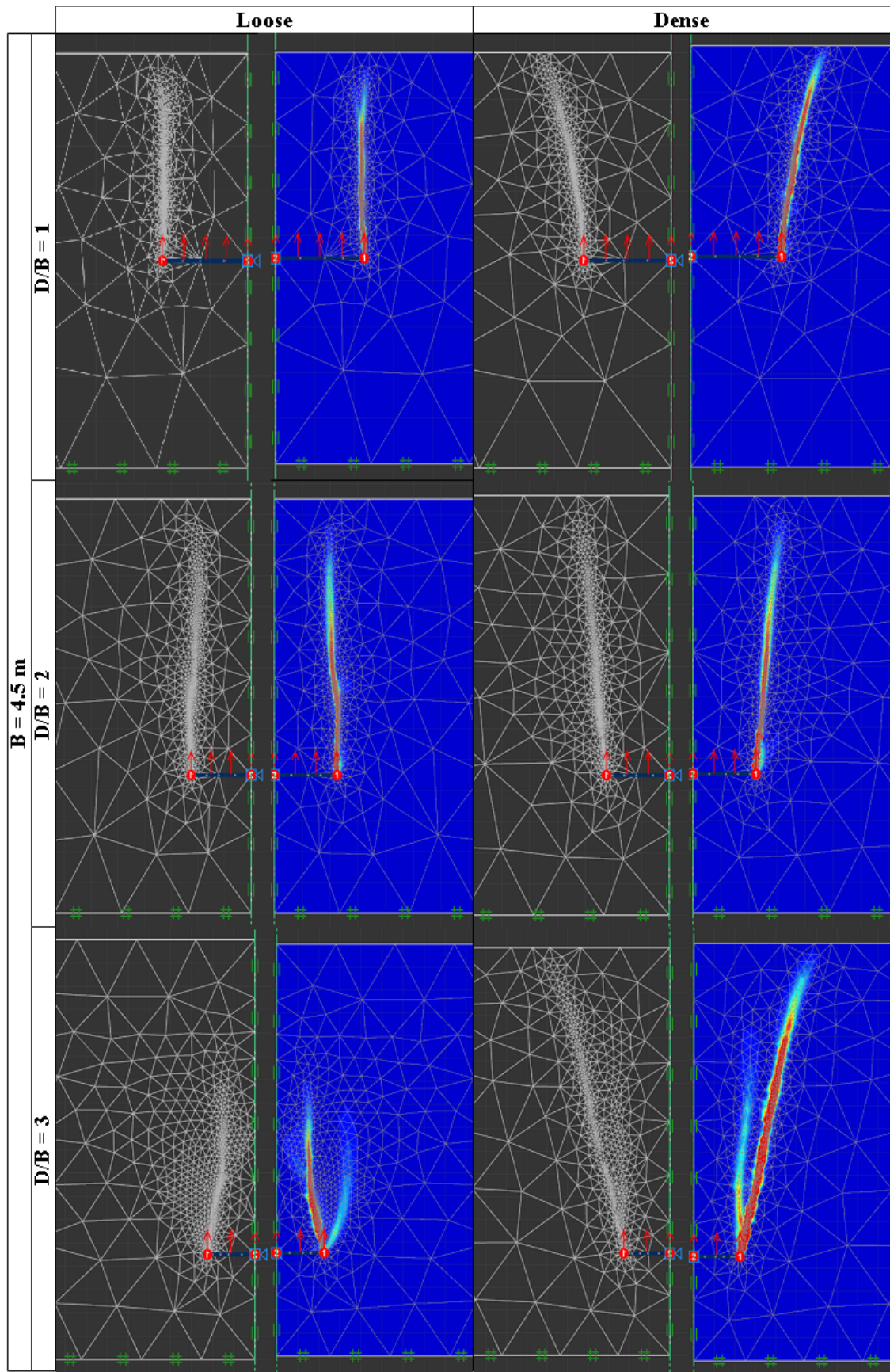


**Figure 3.9:** Shear dissipation of NA model at 10 percent of the maximum value and  $B = 4.5\text{m}$

### 3. Result

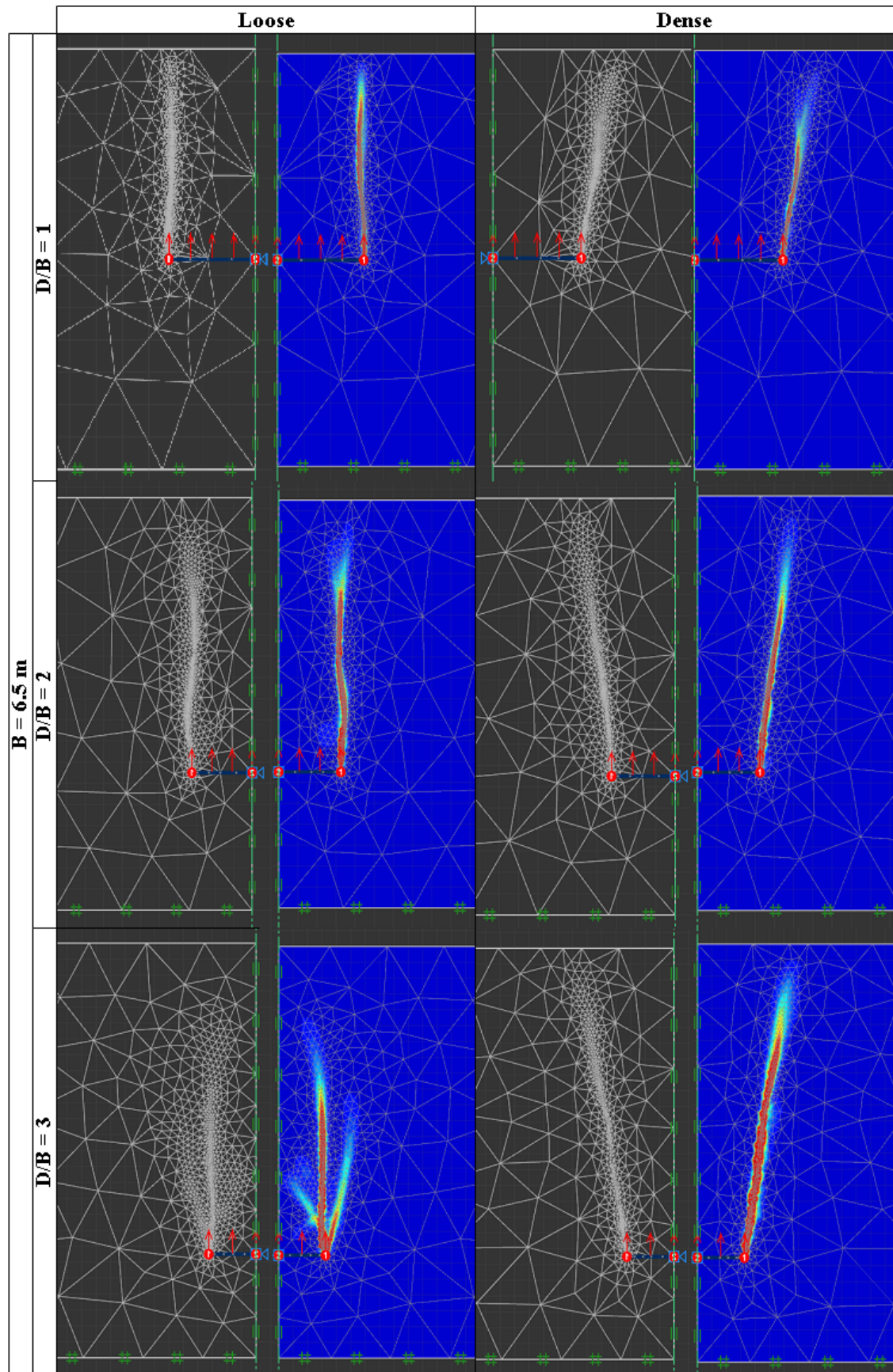


**Figure 3.10:** Shear dissipation of NA model at 10 percent of the maximum value and  $B = 6.5\text{m}$

### 3. Result

## 3.2 Comparison with Previous Researchers

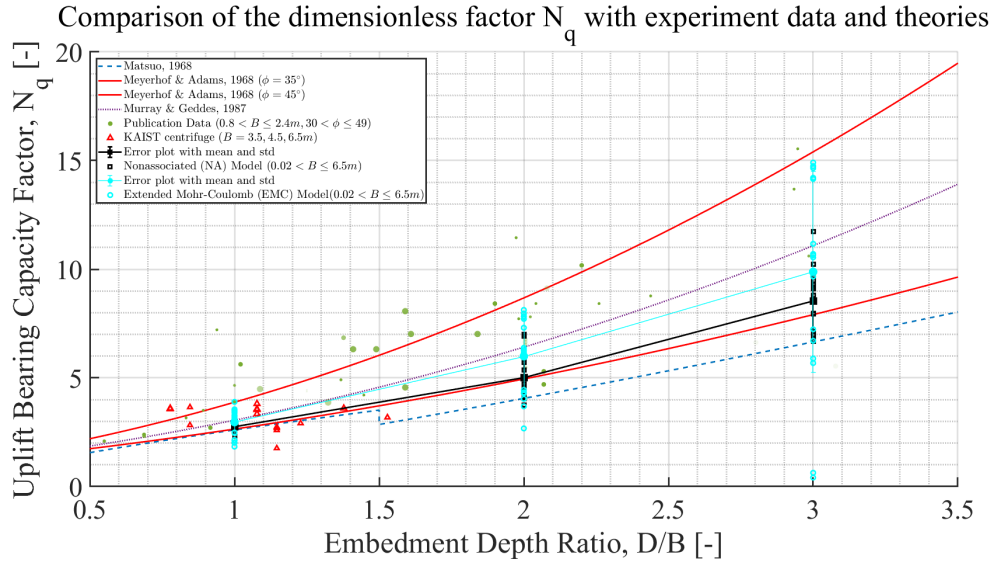


**Figure 3.11:** Comparison with theories and experimental data in all densities of sands

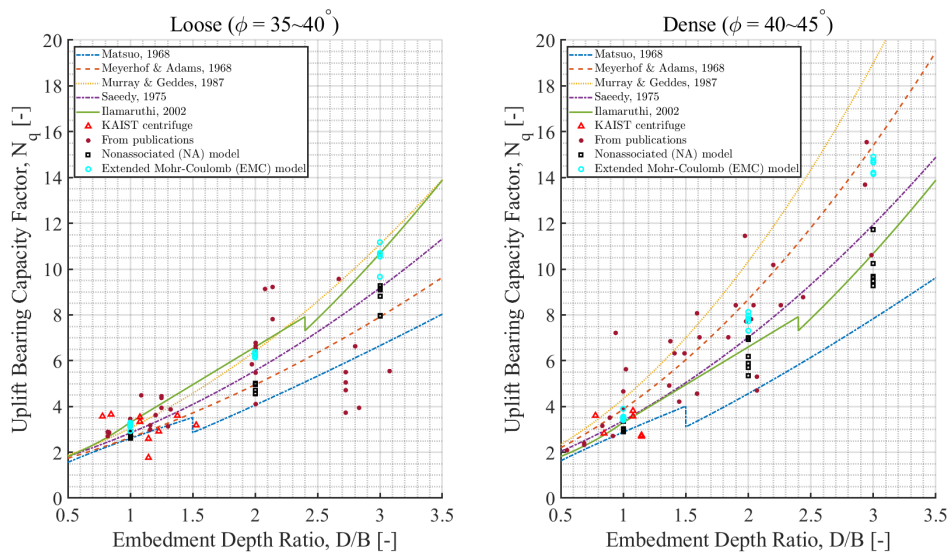


**Figure 3.12:** Comparison with theories and experimental data in loose and dense sands

### 3. Result

#### Comparison of the plot of the effect of width on resistance

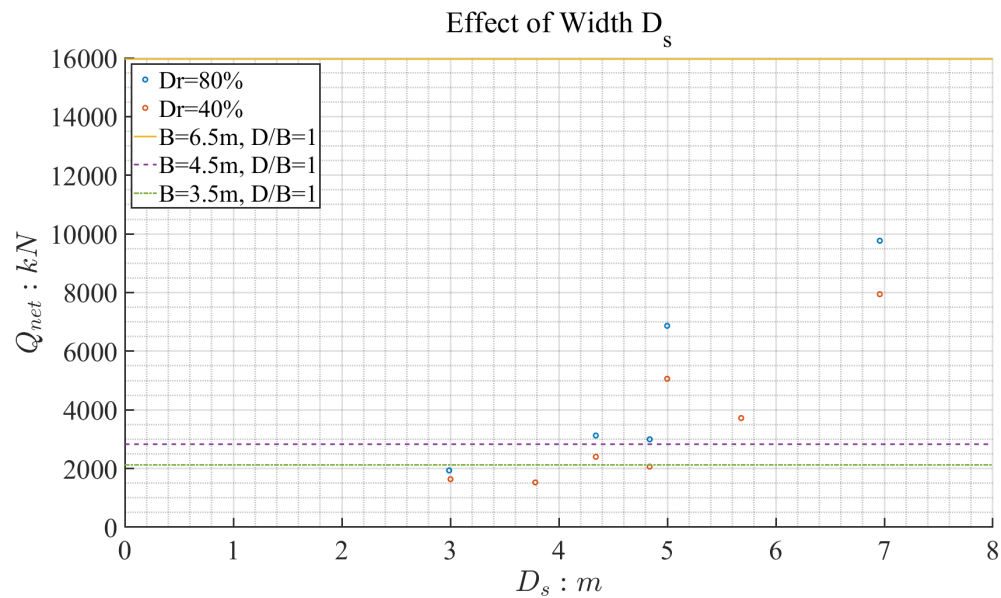


**Figure 3.13:** Comparison drawn

# 4

Comparison with Centrifuge Experiment

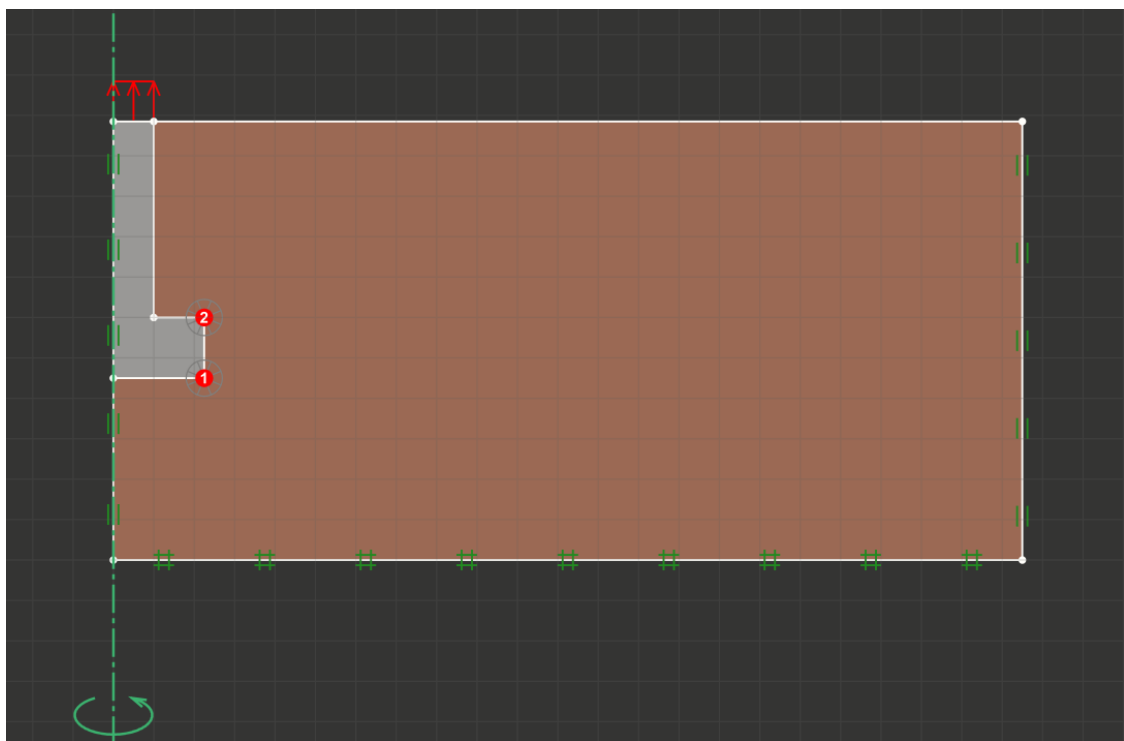


**Figure 4.1:** Typical numerical test set-up

#### 4. Comparison with Centrifuge Experiment

**Table 4.1:** Set of varied model parameters of EMC model

| EMC                    |        |        |        |        |        |
|------------------------|--------|--------|--------|--------|--------|
| Set                    | A      | B      | C      | D      | E      |
| $E_{50}(MPa)$          | 25     | 20     | 22.5   | 35     | 40     |
| $E_{ur}(MPa)$          | 75     | 60     | 67.5   | 105    | 120    |
| $\nu_{ur}$             | 0.3    | 0.3    | 0.3    | 0.3    | 0.3    |
| $c(kPa)$               | 0      | 0      | 0      | 0      | 0      |
| $\phi(deg)$            | 37     | 34     | 35.5   | 38     | 40     |
| $\psi(deg)$            | 11     | 1      | 5      | 8      | 14     |
| $\gamma_d(kN/m^3)$     | 16     | 15.5   | 15.75  | 16.5   | 17     |
| $\gamma_{sat}(kN/m^3)$ | 20     | 19     | 19.5   | 20.5   | 21     |
| $K_0$                  | 0.4264 | 0.4264 | 0.4264 | 0.4264 | 0.4264 |
| $p_{ref}(kPa)$         | 100    | 100    | 100    | 100    | 100    |
| $m$                    | 0.5    | 0.5    | 0.5    | 0.5    | 0.5    |

**Table 4.2:** Set of varied model parameters for NA model

| NA                     |        |        |        |        |        |
|------------------------|--------|--------|--------|--------|--------|
| Set                    | F      | G      | H      | I      | J      |
| $E(MPa)$               | 25     | 20     | 30     | 35     | 40     |
| $\nu$                  | 0.25   | 0.25   | 0.25   | 0.25   | 0.25   |
| $c(kPa)$               | 0      | 0      | 0      | 0      | 0      |
| $\phi(deg)$            | 35     | 33     | 37     | 39     | 41     |
| $\psi(deg)$            | 5      | 4      | 6      | 7      | 8      |
| $\gamma_d(kN/m^3)$     | 16     | 14     | 15     | 16     | 14     |
| $\gamma_{sat}(kN/m^3)$ | 20     | 19     | 19.5   | 20     | 19     |
| $K_0$                  | 0.4264 | 0.4264 | 0.4264 | 0.4264 | 0.4264 |

#### 4. Comparison with Centrifuge Experiment

**Table 4.3:** Centrifuge test set-up and result

| Case | $B(m)$ | $\frac{D}{B}$ | $\gamma_d(kN/m^3)$ | $Q_u(kN)$ |
|------|--------|---------------|--------------------|-----------|
| 1-1  | 4.5    | 1             | 13.8               | 2959      |
| 1-2  | 4.5    | 1.3           | 13.8               | 3845      |
| 1-3  | 4.5    | 1.3           | 13.8               | 4050      |
| 2-1  | 6.5    | 1             | 14                 | 7433      |
| 2-2  | 6.5    | 1.3           | 14                 | 10440     |
| 2-3  | 6.5    | 1.3           | 14                 | 10590     |
| 3-1  | 4.5    | 1             | 15.3               | 3312      |
| 3-2  | 4.5    | 1.3           | 15.3               | 4554      |
| 3-3  | 4.5    | 1.3           | 15.3               | 4824      |
| 4-1  | 6.5    | 1             | 15.3               | 9331      |
| 4-2A | 6.5    | 1.3           | 15.3               | 12280     |
| 4-3  | 6.5    | 1.3           | 15.3               | 12240     |
| 5-1  | 3.5    | 1.3           | 14                 | 1980      |
| 5-2  | 3.5    | 1.6           | 14                 | 2658      |
| 5-3  | 4.5    | 1.6           | 14                 | 5351      |
| 6-3  | 3.5    | 1.6           | 15.1               | 3616      |

**Table 4.4:** Numerical model set-up for load-displacement curve comparison

| Code  | $B(m)$ | $D - t(m)$ | $D(m)$ | $t(m)$ | $b(m)$ | $A(m^2)$ |
|-------|--------|------------|--------|--------|--------|----------|
| base2 | 6.5    | 5.95       | 7.45   | 1.5    | 1      | 39.1     |
| base3 | 6.5    | 4          | 5.5    | 1.5    | 1      | 39.1     |
| base2 | 6.5    | 5.95       | 7.45   | 1.5    | 1      | 39.1     |
| base3 | 6.5    | 4          | 5.5    | 1.5    | 1      | 39.1     |
| base2 | 6.5    | 5.95       | 7.45   | 1.5    | 1      | 39.1     |
| base2 | 6.5    | 5.95       | 7.45   | 1.5    | 1      | 39.1     |
| base2 | 6.5    | 5.95       | 7.45   | 1.5    | 1      | 39.1     |
| base6 | 4.5    | 2          | 3.5    | 1.5    | 1      | 17.1     |
| base5 | 4.5    | 3.35       | 4.85   | 1.5    | 1      | 17.1     |

4. Comparison with Centrifuge Experiment

**Table 4.4 continued from previous page**

| Code  | $B(m)$ | $D - t(m)$ | $D(m)$ | $t(m)$ | $b(m)$ | $A(m^2)$ |
|-------|--------|------------|--------|--------|--------|----------|
| base5 | 4.5    | 3.35       | 4.85   | 1.5    | 1      | 17.1     |
| base6 | 4.5    | 2          | 3.5    | 1.5    | 1      | 17.1     |
| base5 | 4.5    | 3.35       | 4.85   | 1.5    | 1      | 17.1     |
| base5 | 4.5    | 3.35       | 4.85   | 1.5    | 1      | 17.1     |
| base4 | 4.5    | 4.7        | 6.2    | 1.5    | 1      | 17.1     |
| base8 | 3.5    | 3.55       | 4.3    | 0.75   | 0.6    | 11.1     |
| base7 | 3.5    | 4.6        | 5.35   | 0.75   | 0.6    | 11.1     |

#### 4. Comparison with Centrifuge Experiment

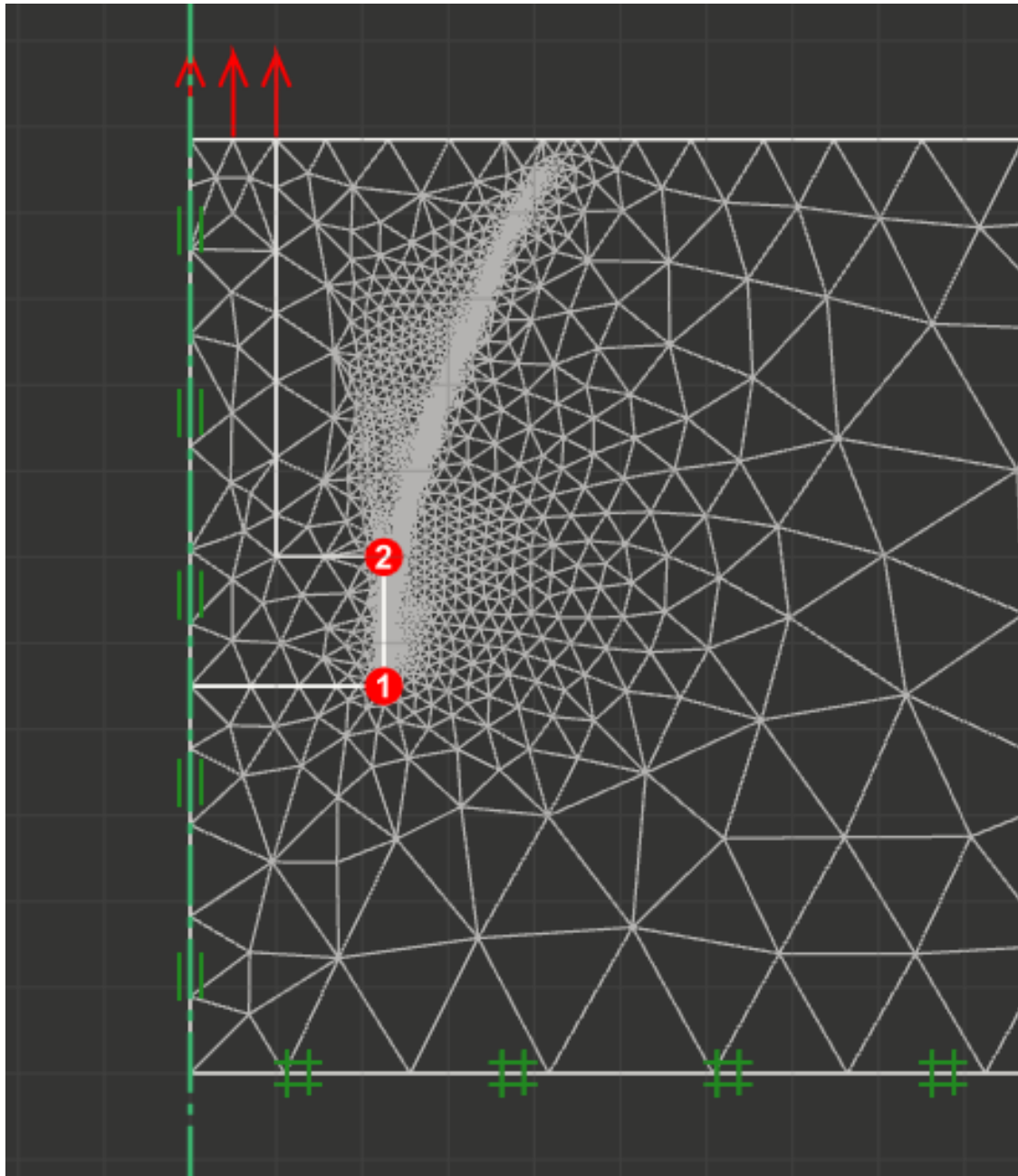


**Figure 4.2:** Typical mesh of the numerical simulation; number of mesh = 5000

#### 4. Comparison with Centrifuge Experiment



**Figure 4.3:** Typical result of the numerical simulation; 1st decile of the shear dissipation (kJ)

#### 4. Comparison with Centrifuge Experiment

Results of numerical analysis for finding the model that fits the centrifuge load—displacement curve

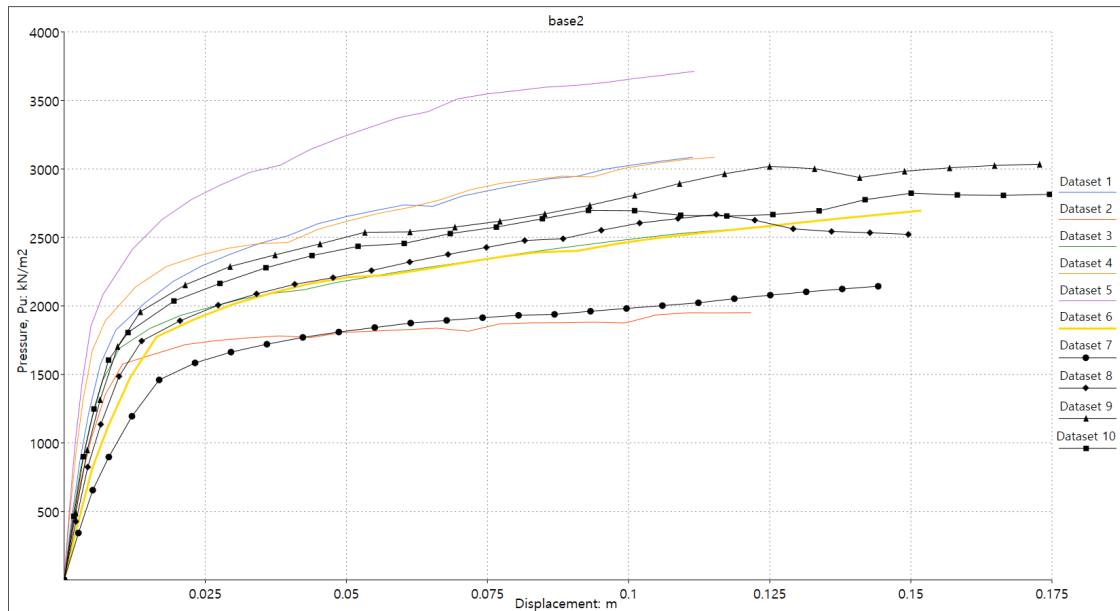


**Figure 4.4:** Code name base2;  $B=6.5m$ ;  $B/D = 0.915$

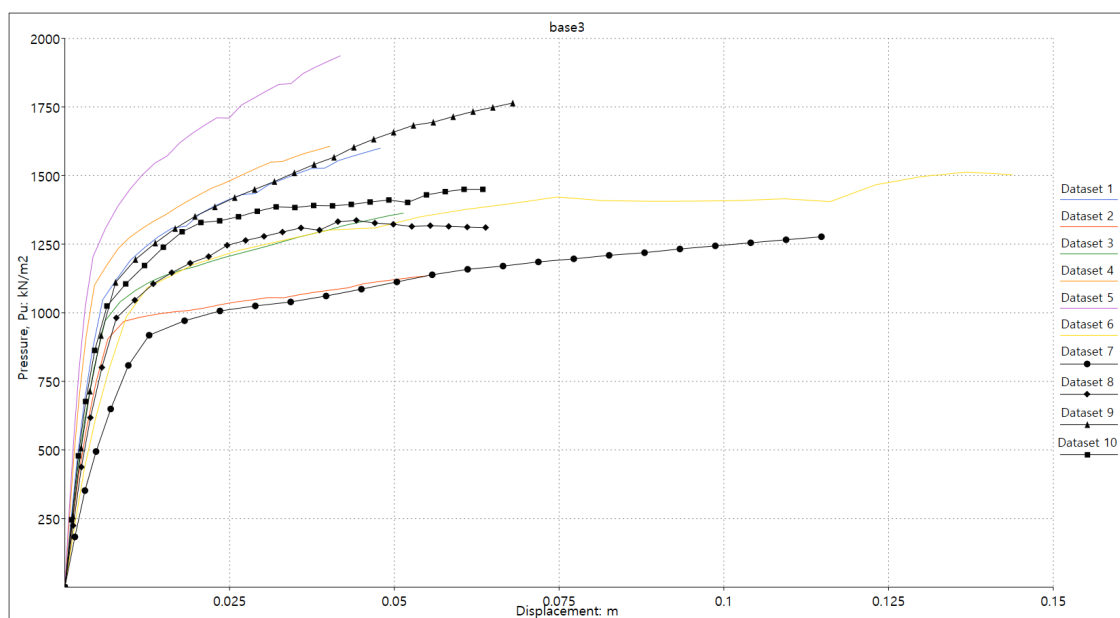


**Figure 4.5:** Code name base3;  $B=6.5m$ ;  $B/D = 0.615$

#### 4. Comparison with Centrifuge Experiment

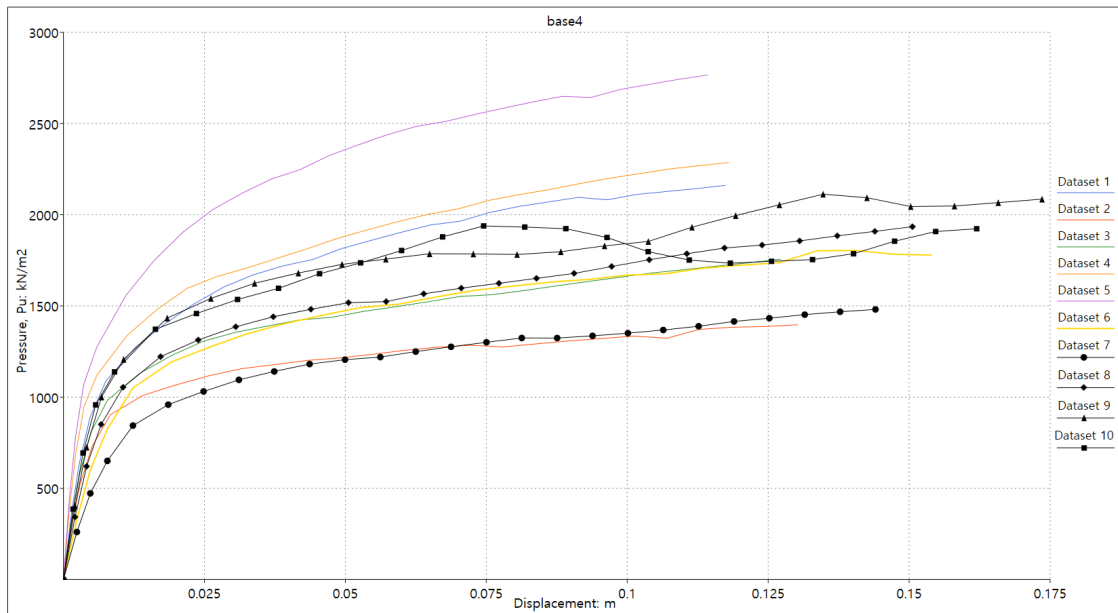


**Figure 4.6:** Code name base4;  $B=4.5\text{m}$ ;  $B/D = 1.044$

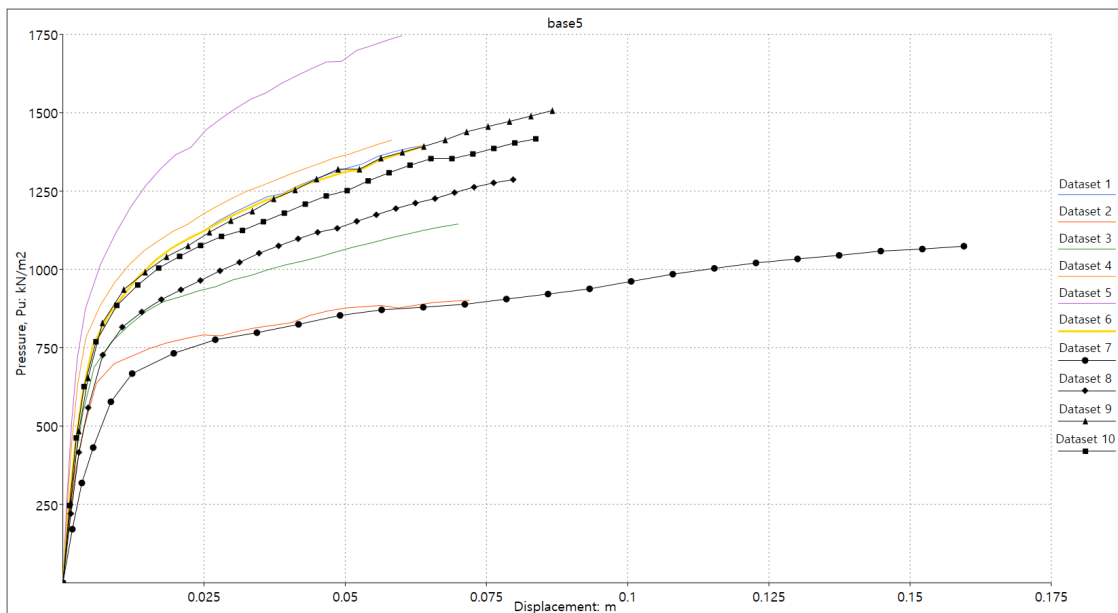


**Figure 4.7:** Code name base5;  $B=4.5\text{m}$ ;  $B/D = 0.744$

#### 4. Comparison with Centrifuge Experiment

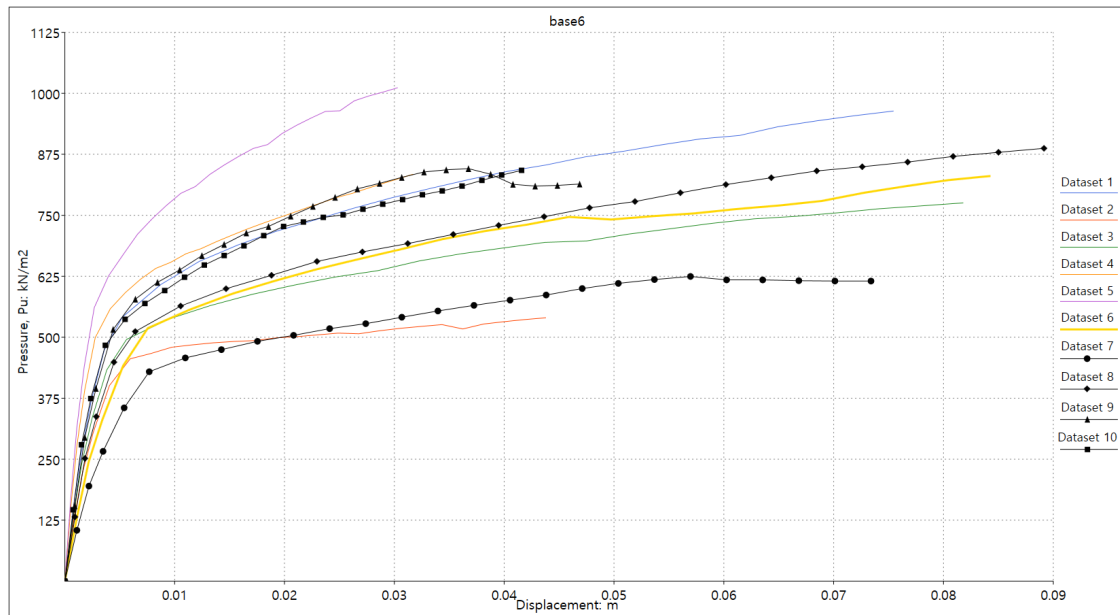


**Figure 4.8:** Code name base6;  $B=4.5\text{m}$ ;  $B/D = 0.444$

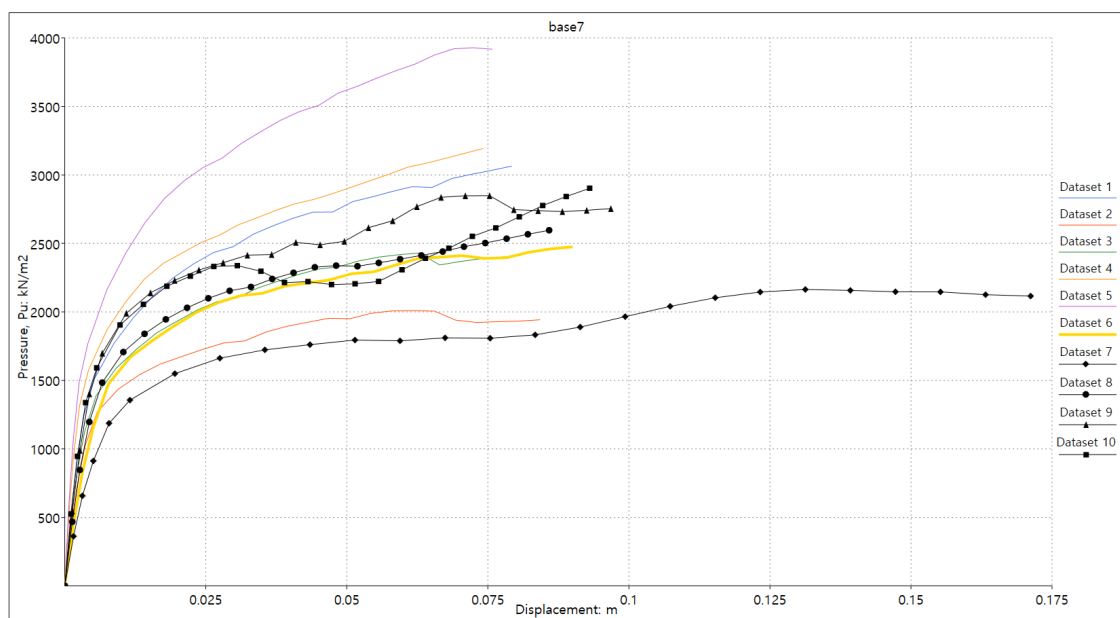


**Figure 4.9:** Code name base7;  $B=3.5\text{m}$ ;  $B/D = 1.314$

#### 4. Comparison with Centrifuge Experiment

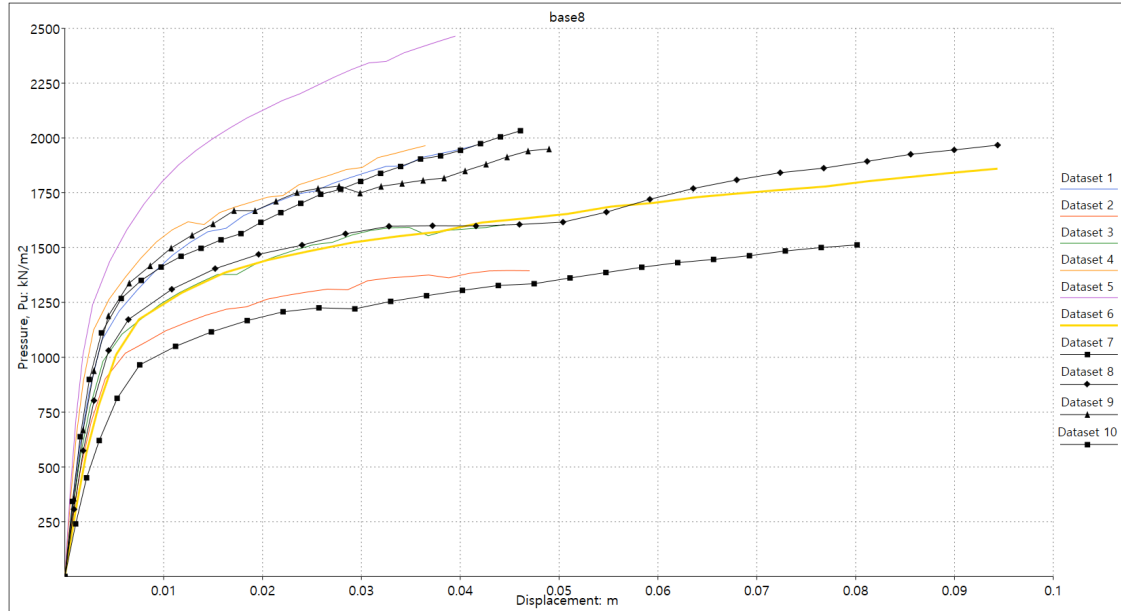


**Figure 4.10:** Code name base8; B=3.5m; B/D = 0.101

#### Determination of model parameters

To evaluate the difference between the centrifuge test result and the model prediction, residual error was used:

$$Error = \left| \frac{y_{actual} - y_{estimated}}{y_{actual}} \right| \times 100\%$$

The goal is to find the model which best fits (or has the least error) the measured data. For the dense sand cases, Model C and H, whereas for the loose sand cases, Model B and G were chosen for the further studies.

#### 4. Comparison with Centrifuge Experiment

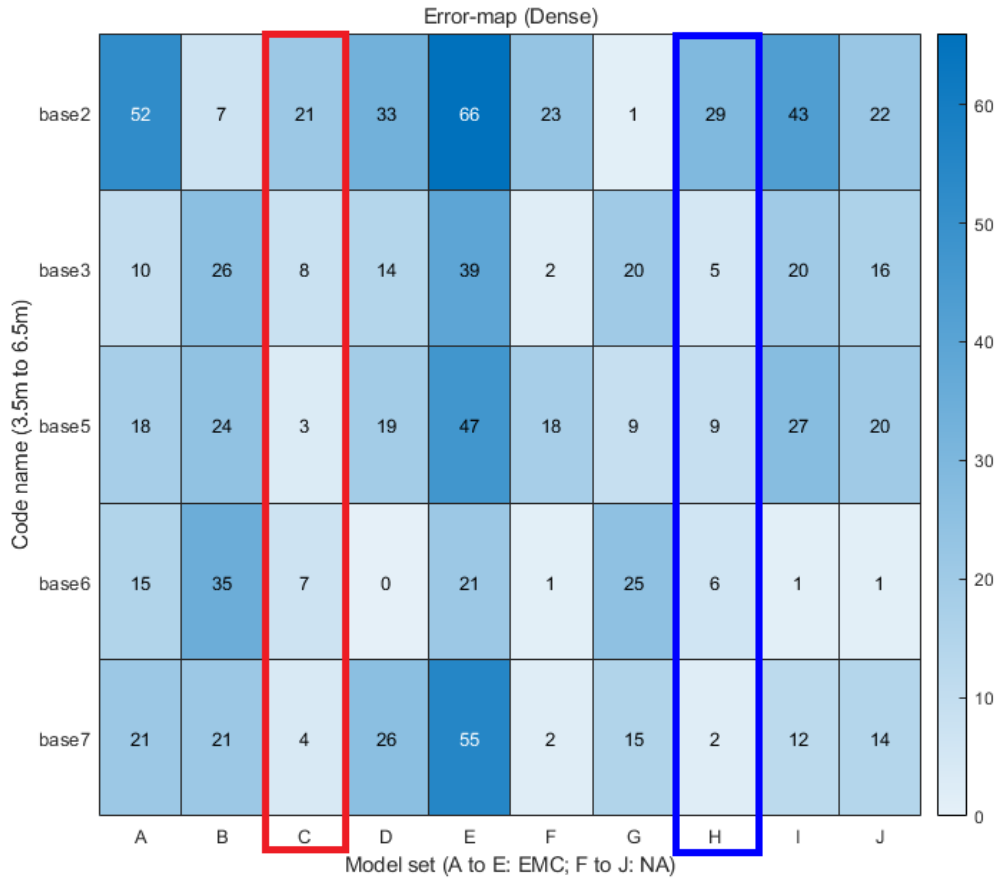


**Figure 4.11:** Heat-map of errors between centrifuge test and model (dense cases); model C and H were selected among available 10 models

#### 4. Comparison with Centrifuge Experiment

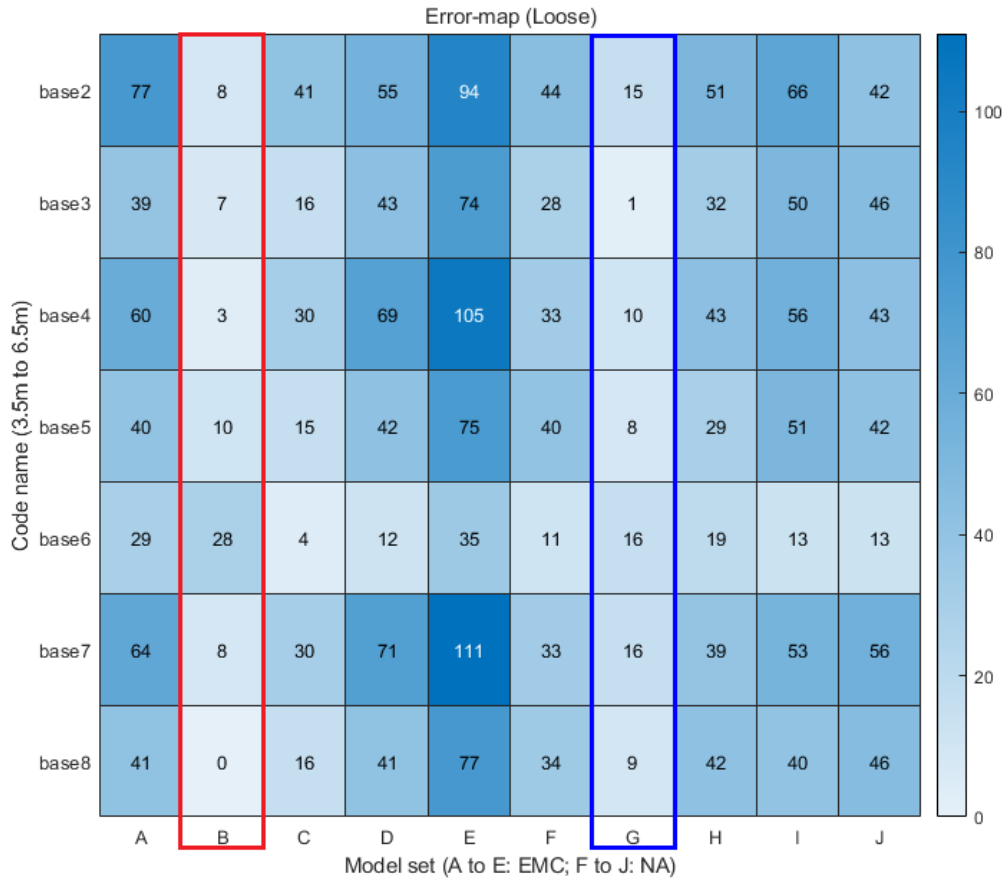


**Figure 4.12:** Heat-map of errors between centrifuge test and model (loose cases); model B and G were selected among 10 available models

4. Comparison with Centrifuge Experiment

## 4.1 Comparison of the centrifuge test results with the chosen model

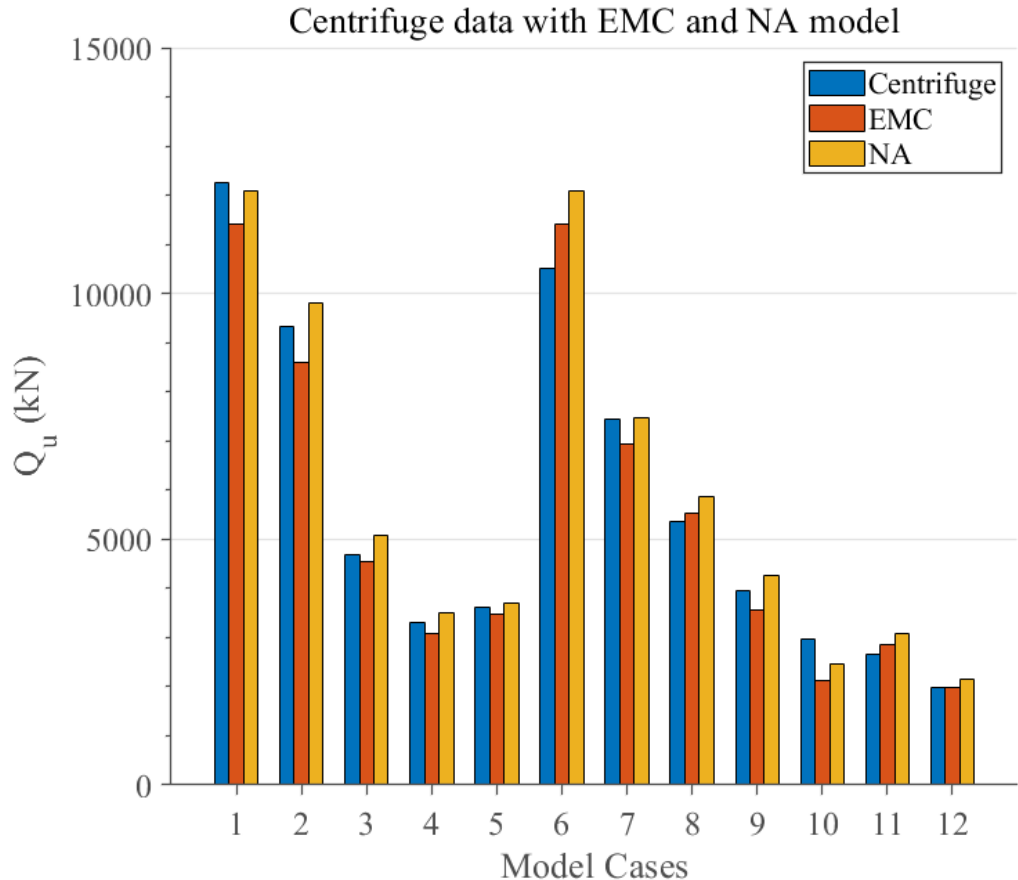


**Figure 4.13:** Bar-chart of centrifuge test and model (all cases); from left to right, 1:  $B=6.5m, D/B=1.3$ ; 2:  $B=6.5m, D/B=1$ ; 3:  $B=4.5m, D/B=1.3$ ; 4:  $B=4.5m, D/B=1$ ; 5:  $B=3.5m, D/B=1.6$ ; 6:  $B=6.5m, D/B=1.3$ ; 7:  $B=6.5m, D/B=1$ ; 8:  $B=4.5m, D/B=1.6$ ; 9:  $B=4.5m, D/B=1.3$ ; 10:  $B=4.5m, D/B=1$ ; 11:  $B=3.5m, D/B=1.6$ ; 12:  $B=3.5m, D/B=1.3$

## Result of load—displacement curves of the centrifuge measurement with EMC and NA models

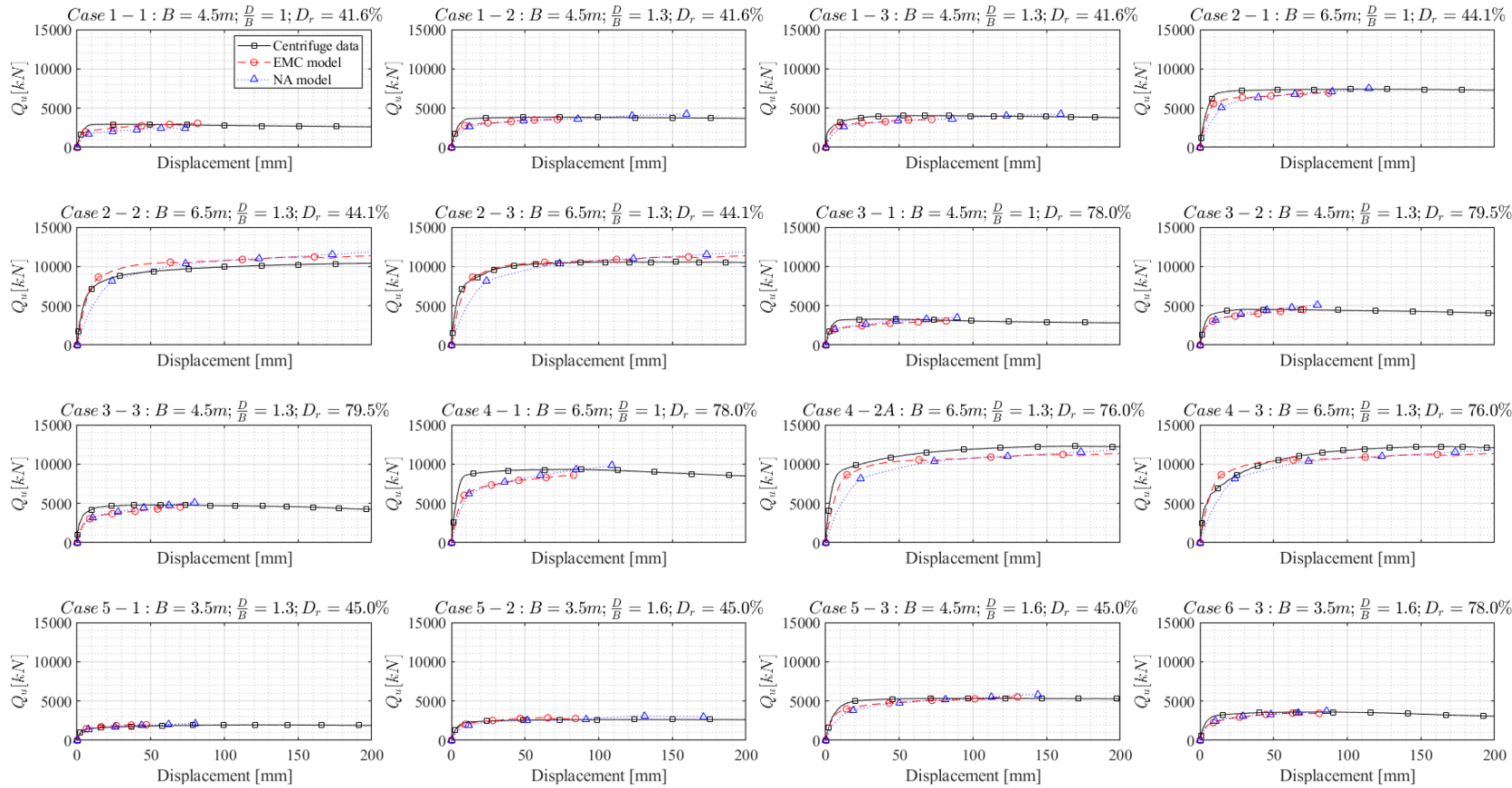
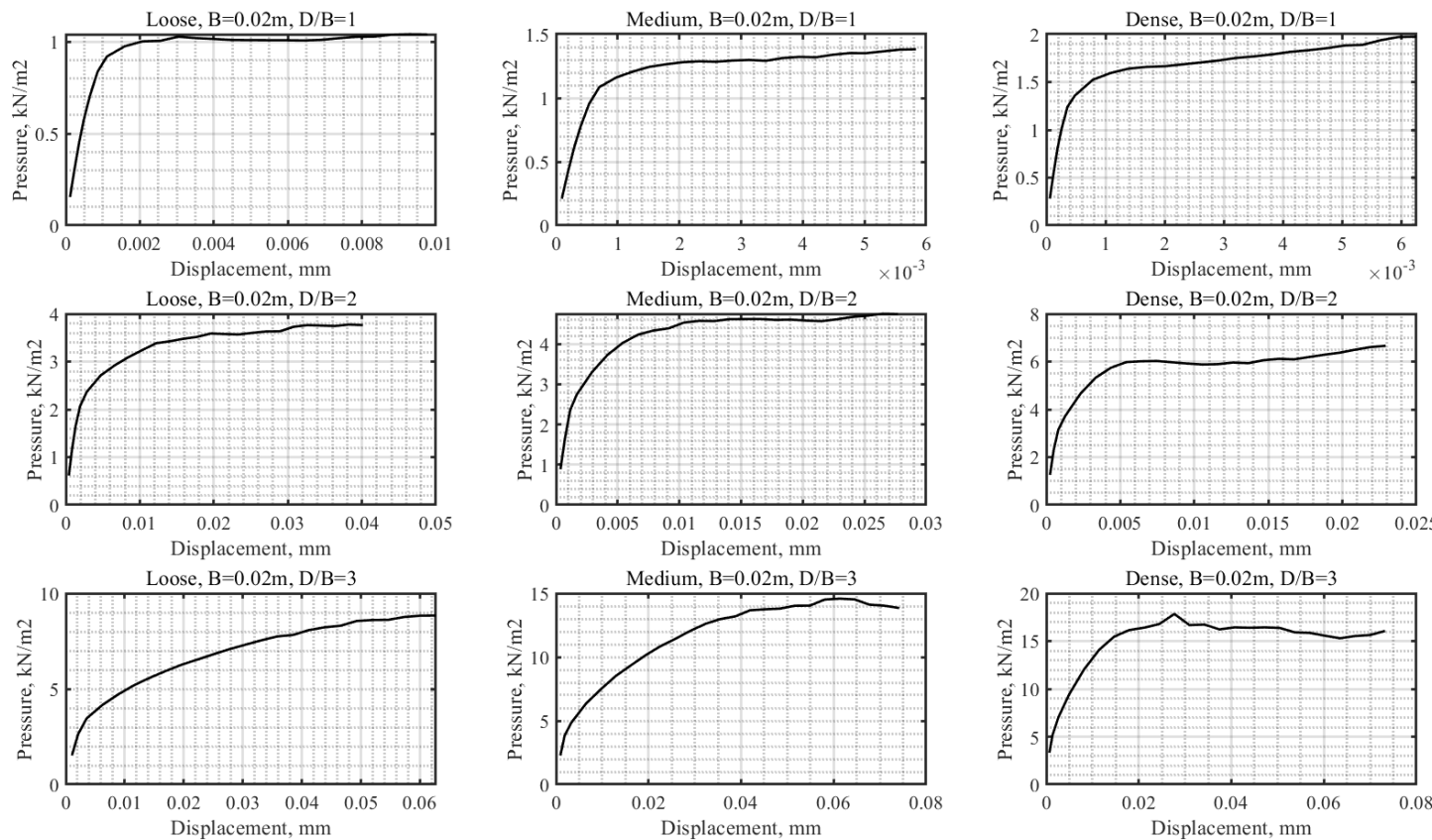


Figure 4.14: Comparison of centrifuge data with EMC and NA models

# Appendices

A

## List of Load—Displacement Curves



**Figure A.1:** Cumulative load-displacement curves of uplift of plate anchor in loose, medium, dense sands; D/B = 1,2,3; B=0.02m

A. List of Load—Displacement Curves

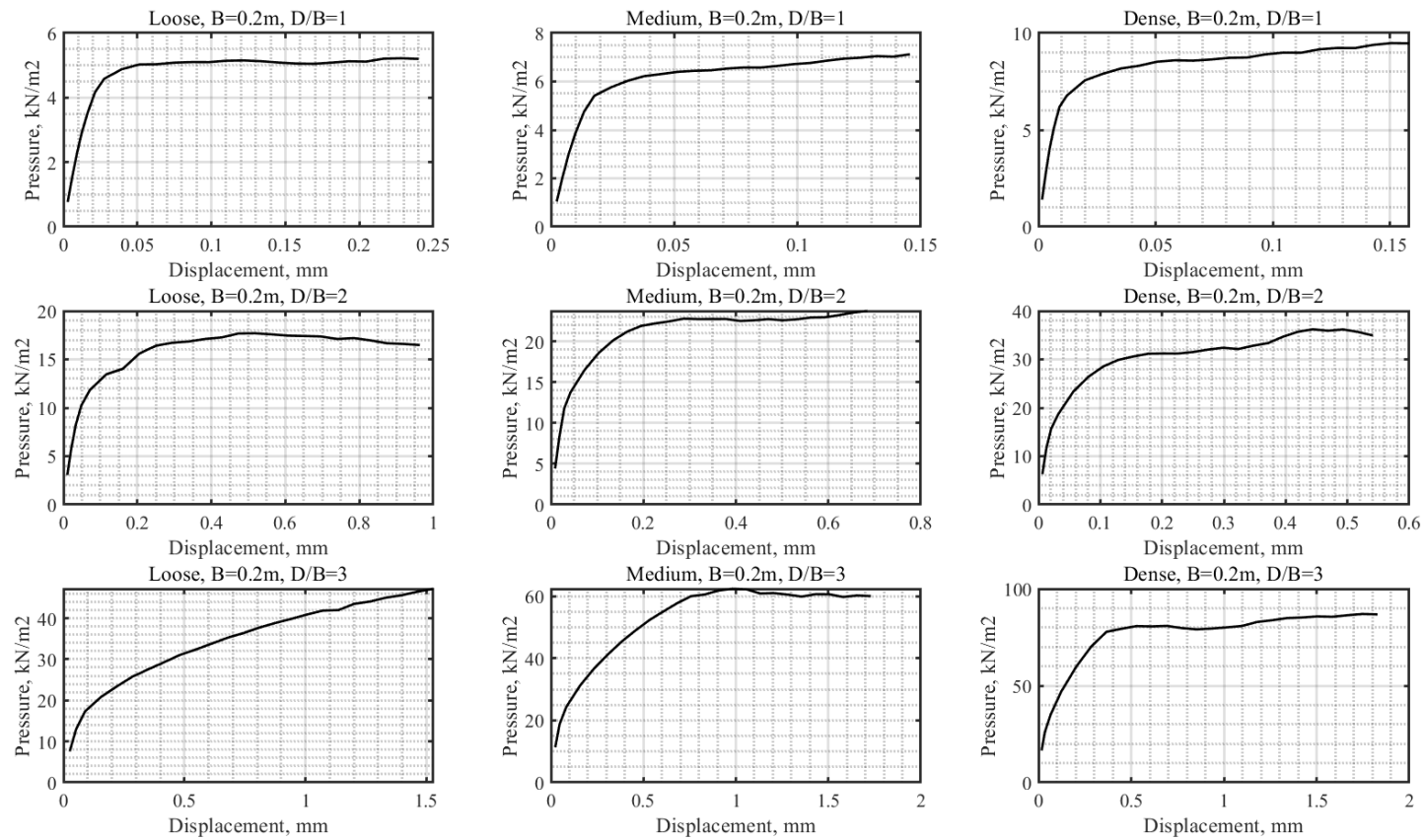


**Figure A.2:** Cumulative load-displacement curves of uplift of plate anchor in loose, medium, dense sands;  $D/B = 1,2,3$ ;  $B=0.2m$

A. List of Load—Displacement Curves

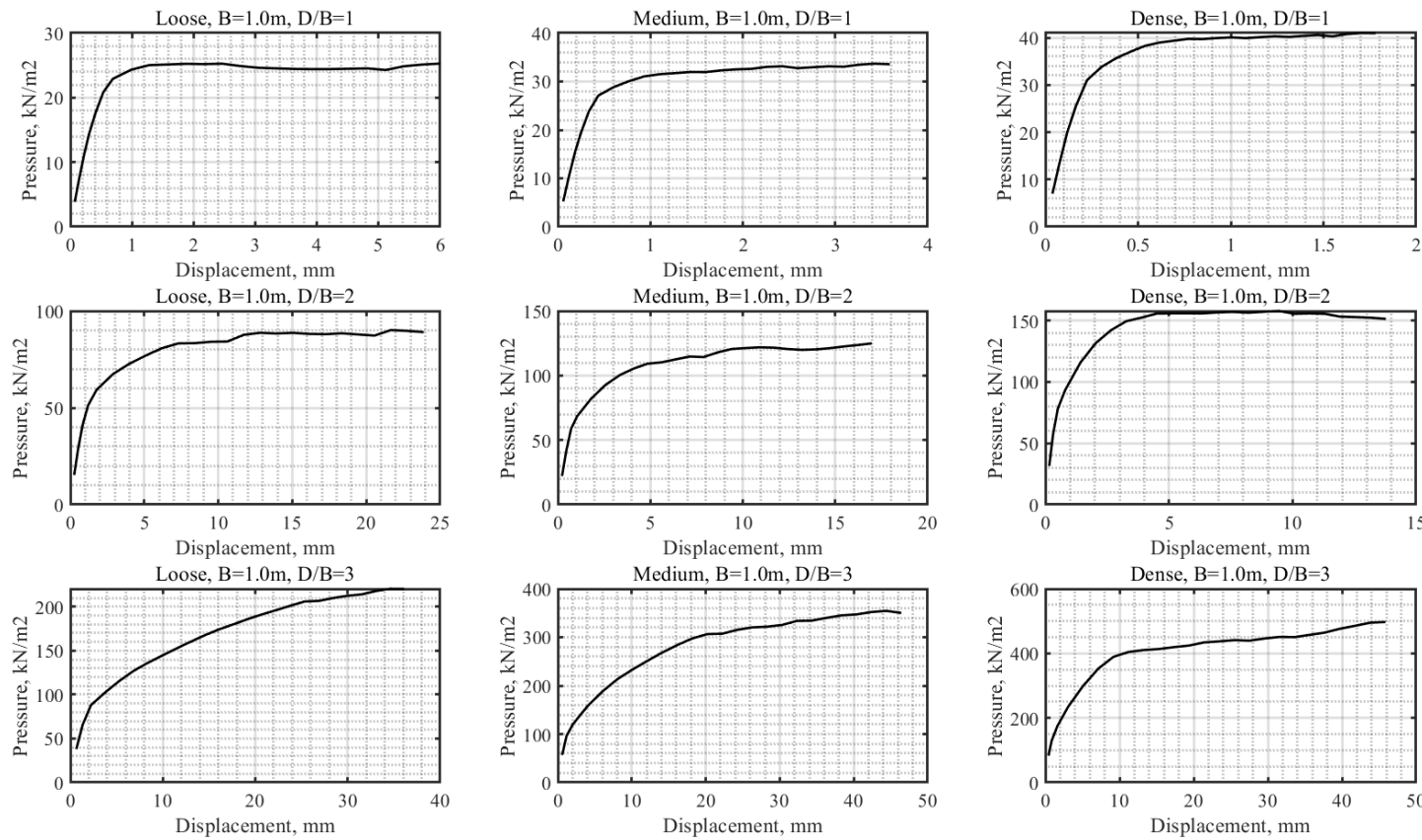


**Figure A.3:** Cumulative load-displacement curves of uplift of plate anchor in loose, medium, dense sands;  $D/B = 1,2,3$ ;  $B=1.0\text{m}$

A. List of Load—Displacement Curves

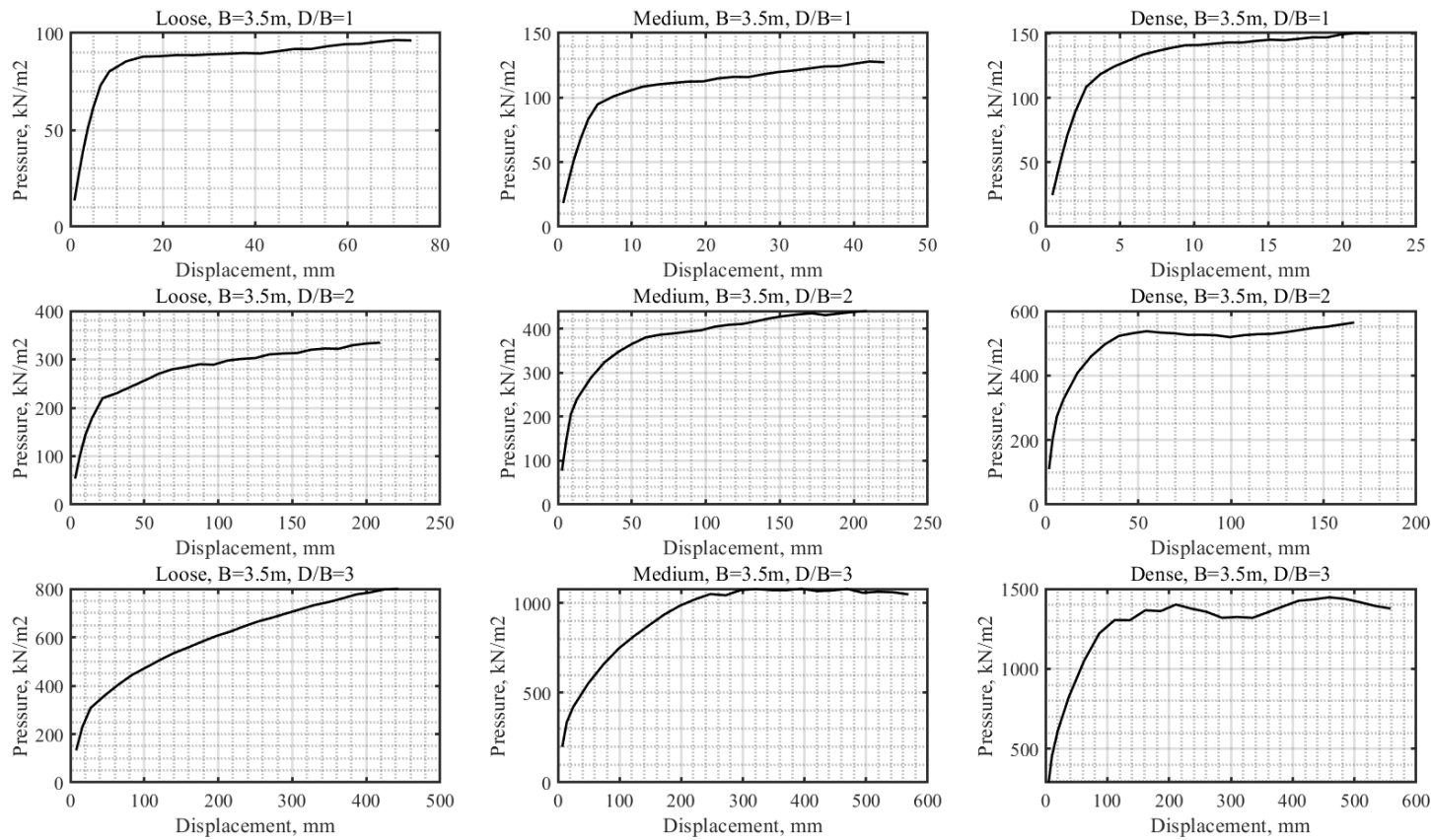


**Figure A.4:** Cumulative load-displacement curves of uplift of plate anchor in loose, medium, dense sands;  $D/B = 1,2,3$ ;  $B=3.5m$

*A. List of Load—Displacement Curves*

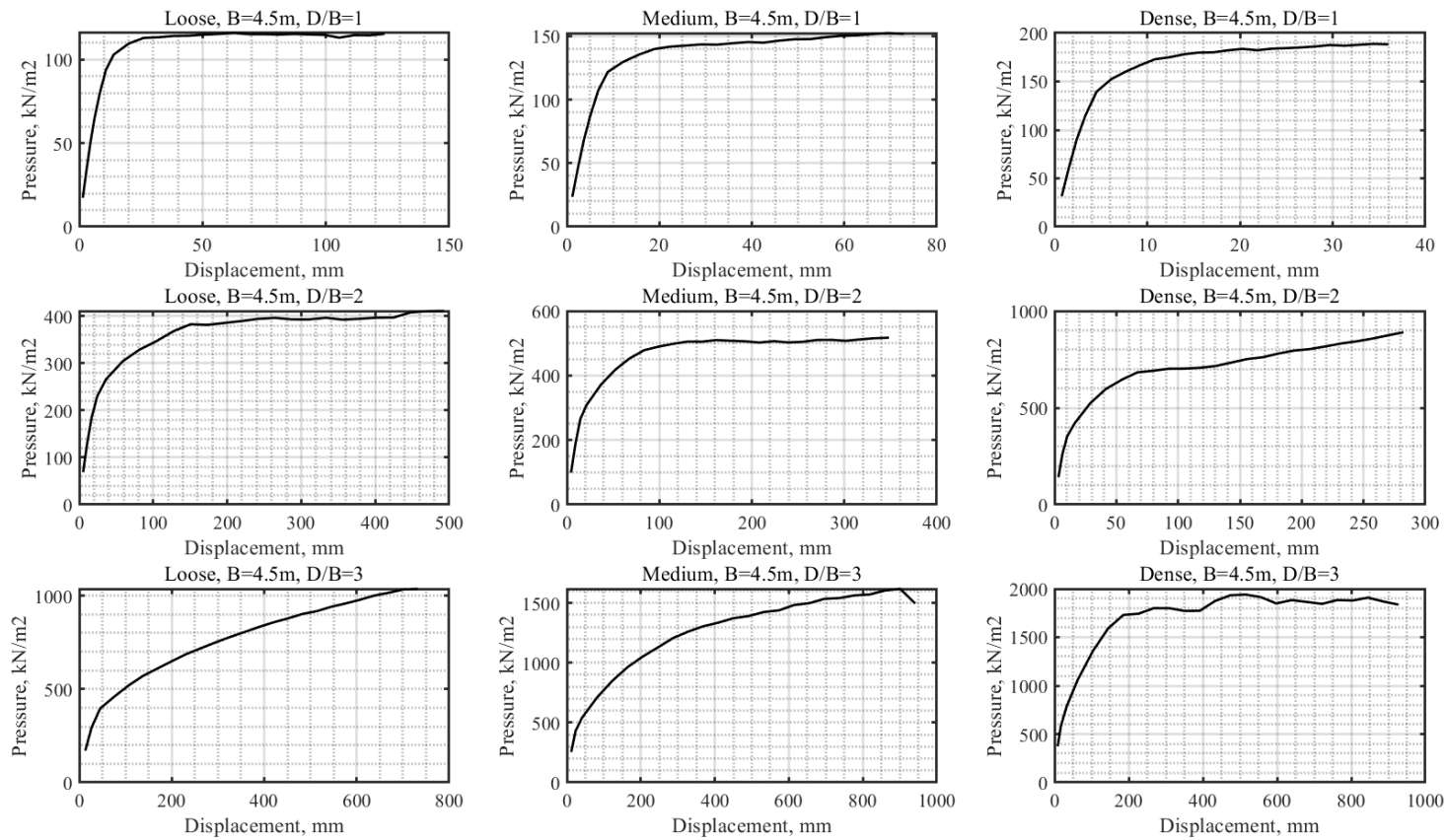


**Figure A.5:** Cumulative load-displacement curves of uplift of plate anchor in loose, medium, dense sands; D/B = 1,2,3; B=4.5m

A. List of Load—Displacement Curves

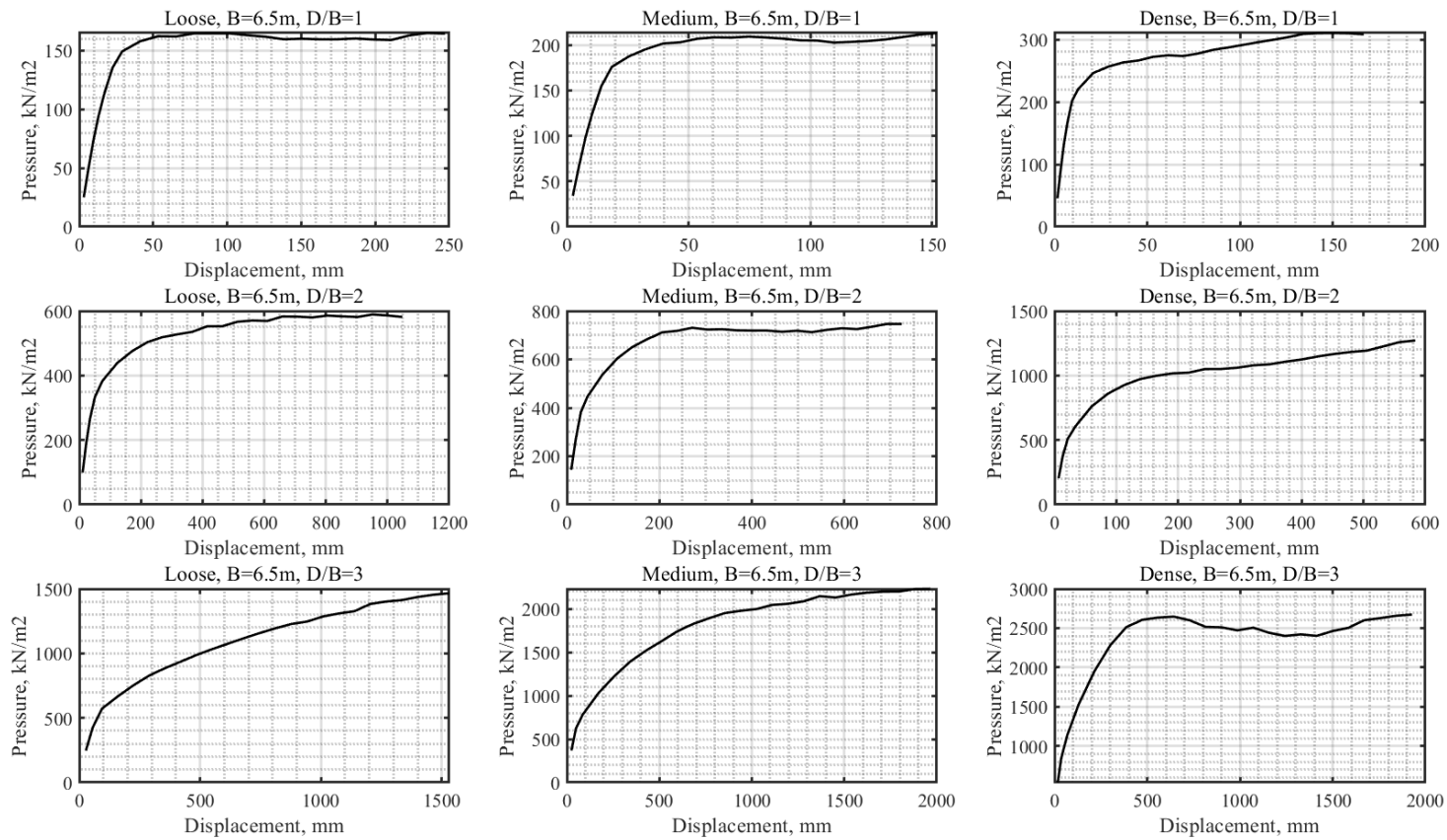


**Figure A.6:** Cumulative load-displacement curves of uplift of plate anchor in loose, medium, dense sands; D/B = 1,2,3; B=6.5m

# B

## REFERENCES

Wood, D. M. (2017). Geotechnical modelling. CRC press.

Doherty, J. P., & Muir Wood, D. (2013). An extended Mohr–Coulomb (EMC) model for predicting the settlement of shallow foundations on sand. *Géotechnique*, 63(8), 661-673.

Gajo, A., & Wood, M. (1999). Severn–Trent sand: a kinematic-hardening constitutive model: the q–p formulation. *Géotechnique*, 49(5), 595-614.

Krabbenhoft, S., Krabbenhoft, K., & Christensen, R. Limit analysis of the bearing capacity of strip-and circular footings on a layer of sand overlying clay.

Sakai, T., & Tanaka, T. (2007). Experimental and numerical study of uplift behavior of shallow circular anchor in two-layered sand. *Journal of geotechnical and geoenvironmental engineering*, 133(4), 469-477.

Tanaka, T., & Sakai, T. (1993). Progressive failure and scale effect of trap-door problems with granular materials. *Soils and Foundations*, 33(1), 11-22.

Sakai, T., & Tanaka, T. (1998). Scale effect of a shallow circular anchor in dense sand. *Soils and Foundations*, 38(2), 93-99.

## B. REFERENCES

- Sakai, T., & Tanaka, T. (2007). Experimental and numerical study of uplift behavior of shallow circular anchor in two-layered sand. *Journal of geotechnical and geoenvironmental engineering*, 133(4), 469-477.
- Riyad, A. S. M., Rokonuzzaman, M., & Sakai, T. (2020). Progressive failure and scale effect of anchor foundations in sand. *Ocean Engineering*, 195, 106496.
- Kumar, J., & Kouzer, K. M. (2008). Vertical uplift capacity of horizontal anchors using upper bound limit analysis and finite elements. *Canadian Geotechnical Journal*, 45(5), 698-704.
- Riyad, A. S. M., Rokonuzzaman, M., & Sakai, T. (2020). Effect of using different approximation models to the exact Mohr–Coulomb material model in the FE simulation of Anchor Foundations in sand. *International Journal of Geo-Engineering*, 11(1), 1-21.
- Riyad, A. S. M., Rokonuzzaman, M., & Sakai, T. (2020). Progressive failure and scale effect of anchor foundations in sand. *Ocean Engineering*, 195, 106496.
- Roy, A., Chow, S. H., O'Loughlin, C. D., & Randolph, M. F. (2021). Towards a simple and reliable method for calculating uplift capacity of plate anchors in sand. *Canadian Geotechnical Journal*, 58(9), 1314-1333.